Massive invasion of organellar DNA drives nuclear genome evolution in *Toxoplasma*

Sivaranjani Namasivayam[a,1], Cheng Sun[b,1] Assiatu B Bah[c], Jenna Oberstaller[d], Edwin Pierre-Louis[e], Ronald Drew Etheridge[e], Cedric Feschotte[f], Ellen J. Pritham[c,2] and Jessica C. Kissinger[g,2]

[a]Department of Genetics, University of Georgia, Athens, GA 30602, USA; Present address: Clinical Microbiome Unit, Laboratory of Host Immunity and Microbiome, NIAID, NIH, Bethesda, MD 20892, USA

[b]Department of Biology, University of Texas at Arlington, Arlington, TX 76019, USA; Present address: College of Life Sciences, Capital Normal University, Beijing 100048, China

[c]Department of Biology, University of Texas at Arlington, Arlington, TX 76019

[d]Department of Genetics, University of Georgia, Athens, GA 30602, USA; Present address: Department of Global Health, University of South Florida, Tampa, FL 33620, USA

[e]Department of Cellular Biology, Center for Tropical and Emerging Global Diseases, University of Georgia, Athens, GA 30602, USA

[f]Department of Biology, University of Texas at Arlington, Arlington, TX 76019; Present address: Department of Molecular Biology and Genetics, Cornell University, Ithaca, NY 14853-2703, USA

[g]Department of Genetics, Institute of Bioinformatics, and Center for Tropical and Emerging Global Diseases, University of Georgia, Athens, GA 30602, USA

[1]S.N. and C.S contributed equally to this work
[2]To whom correspondence should be addressed

Email: jkissing@uga.edu

Author Contributions: EJP, JCK and CF designed and supervised the research; SN, CS, AB, JO, EPL and RDE performed the research; SN, CS, EJP, JCK, and RLP analyzed data; SN, CS, CF, JCK and EJP wrote the paper.

Competing Interest Statement: The authors declare no competing interests.

Keywords: Nuclear integrants of Mitochondrial DNA - NUMTs, Nuclear integrants of Plastid DNA - NUPTs, Nuclear DNA of organellar origin - NUOT, Coccidia, Non-Homologous End-Joining repair - NHEJ

This PDF file includes:

Main Text
Figures 1 to 4
Tables 1

Abstract

Toxoplasma gondii is a zoonotic protist pathogen that infects up to 1/3 of the human population. This apicomplexan parasite contains three genome sequences: nuclear (63 Mb); plastid organellar, ptDNA (35 kb); and mitochondrial organellar, mtDNA (5.9 kb of non-repetitive sequence). We find that the nuclear genome contains a significant amount of NUMTs (nuclear DNA of mitochondrial origin) and NUPTs (nuclear DNA of plastid origin) that are continuously acquired and represent a significant source of intraspecific genetic variation. NUOT (nuclear DNA of organellar origin) accretion has generated 1.6% of the extant *T. gondii* ME49 nuclear genome; the highest fraction ever reported in any organism. NUOTs are primarily found in organisms that retain the non-homologous end-joining repair pathway. Significant movement of organellar DNA was experimentally captured via amplicon sequencing of a CRISPR-induced double-strand break in non-homologous end-joining repair competent, but not *ku80* mutant, *Toxoplasma* parasites. Comparisons with *Neospora caninum*, a species that diverged from *Toxoplasma* ~28 MY ago, revealed that the movement and fixation of 5 NUMTs predates the split of the two genera. This unexpected level of NUMT conservation suggests evolutionary constraint for cellular function. Most NUMT insertions reside within (60%) or nearby genes (23% within 1.5 kb) and reporter assays indicate that some NUMTs have the ability to function as cis-regulatory elements modulating gene expression. Together these findings portray a role for organellar sequence insertion in dynamically shaping the genomic architecture and likely contributing to adaptation and phenotypic changes in this important human pathogen.

Significance Statement

This study reveals how DNA located in cellular compartments called organelles can be transferred to the nucleus of the cell and inserted into the nuclear genome of apicomplexan parasite *Toxoplasma*. Insertions alter the DNA sequence and may lead to significant changes in how genes function. Unexpectedly, we found that the human protist pathogen, *Toxoplasma gondii* and closely-related species have the largest observed organellar genome fragment content (>11,000 insertion comprising over 1 Mb of DNA) inserted into their nuclear genome sequence despite their compact 65 Mb nuclear genome. Insertions are occurring at a rate that makes them a significant mutational force that deserves further investigation when examining causes of adaptation and virulence of these parasites.

Introduction

Toxoplasma gondii is a cosmopolitan apicomplexan protist parasite (Fig. 1A), capable of infecting nearly all warm-blooded animals including humans (1, 2). *T. gondii* causes toxoplasmosis, and the parasite infects as much as one third of the world's human population with individual countries showing infection rates ranging from 10 to 80% (3). While the parasite rarely causes symptoms in healthy adults, it can lead to serious and even life-threatening illness in immunosuppressed or pregnant individuals (4, 5). Phylogenetic and population studies of *T. gondii* reveal an unusual population structure consisting of mostly clonal lineages that occasionally recombine (6-9) as well as the recent evolution of oral infectivity that permits the parasite to spread asexually via consumption of tissue cyst forms in addition to traditional transmission of sexually derived oocysts in the environment via a fecal/oral route (10). While it is clear that *Toxoplasma* and other coccidian parasites evolve and adapt rapidly, little is known about the source(s) of genomic variation driving adaptation in *Toxoplasma*. The ability of *Toxoplasma* to propagate asexually, combined with the observed low levels of sexual recombination in existing data and the lack of detectable mobile elements create real challenges for *Toxoplasma* with respect to sources of genomic variation. When contemplating genome evolution and the differences between strains and species it is common practice to examine single nucleotide polymorphisms (SNPs), insertion/deletion events (indels), rearrangements, horizontal and intracellular gene transfers and transposable element (TE) insertion or movement. The insertion of random fragments of organellar DNA is not high on the list of features examined as a major cause of phenotypic or genotypic diversity, but if the organism is a tissue coccidian like *Toxoplasma*, perhaps it should be.

In eukaryotes, DNA of endosymbiotic organelles (mitochondria and chloroplasts) has been observed to be transferred to the nuclear genome (11). During the early phase of organelle

evolution, this process resulted in a massive relocation of entire organellar genes to the nuclear genome (12). In many eukaryotes, the transfer of functional organellar genes appears rare or has ceased altogether (13, 14), and almost all recent transfers of mitochondrial (mtDNA) or plastid (ptDNA) DNA to the nuclear genome are gene or genome fragments that give rise to noncoding sequences, called NUMTs (nuclear integrants of mtDNA) and NUPTs (nuclear integrants of ptDNA). Organellar-to-nuclear DNA transfer has been reported for 85 fully sequenced eukaryotic genomes and fully characterized in 23 mammals (15). The results are indicative of the significant driving force NUOTs (nuclear DNA of organellar origin) provide for gene and genome innovation in eukaryotes (11) including humans (16) and other primates (17, 18). In *Saccharomyces cerevisiae*, 16 NUMTs were unexpectedly recovered in a double-strand break experiment (19) and the non-homologous end-joining repair pathway, NHEJ, was shown to be the mechanism responsible for NUMT integration (19, 20). Mechanistically, reactive oxygen species (ROS) can generate double-stranded mtDNA breaks (DSBs) and mtDNA fragments (21) and there are hypotheses and some evidence for how organellar DNA, in particular mtDNA may enter the host nucleus and be used to patch nuclear DSBs (22).

Nuclear genome sequences in the Apicomplexa are highly streamlined, ranging from 8 to 130 Mb, dynamic in structure and rapidly evolving (23, 24). Transposable elements (TEs), which generally constitute the most significant proportion of repetitive DNA in genomes and are known to be powerful agents for generating genomic plasticity (25, 26), are absent from most apicomplexans examined thus far (27) excepting the genera *Ascogregarina*, *Eimeria* and *Sarcocystis* (28, 29). Consequently, it is of interest to understand what factors contribute to the generation of genomic plasticity in apicomplexan parasites. While organellar-to-nuclear DNA transfer represents a significant driving force for genome innovation in eukaryotes, it has not been examined in apicomplexans (outside of nuclear-encoded, organellar-targeted proteins) (30, 31), and little is known about the evolutionary fate and consequence of these transferred DNA sequences.

Most apicomplexans contain two organelles, a mitochondrion and a plastid (pt) called the apicoplast that was acquired through the secondary endosymbiosis of a red alga (32-34). The ptDNA sequence (35 kb) is a circular/cruciform structure and is well conserved across apicomplexans (35). The mtDNA sequences generated thus far are variable and occur as linear monomers (~6 kb) or concatemers with, or without, inverted repeats depending on the species (36, 37). Despite the genome topological differences, the apicomplexan mtDNA consistently encodes three cytochrome genes: cytochrome oxidase subunits I and III (*coxI, coxIII)* and cytochrome b (*cob*) and highly fragmented large and small subunit rRNA genes (LSU – SSUrRNA) (36, 37). Unlike the ptDNA sequence, the mtDNA sequence of *T. gondii* remained elusive until recently (36). It is structurally divergent and consists of 21 unique sequence blocks (SBs) that represent highly fragmented protein coding and rRNA genes (36). These sequence blocks are highly redundant, as was observed in dinoflagellates (38, 39). The presence of NUMTs in *Toxoplasma* was first reported as REP elements in 1991 (40), but they have not been studied since. The availability of genome sequences for numerous *Toxoplasma* strains as well as organellar DNA sequences, permitted a systematic examination of NUOTs in *T. gondii* and its relatives to shed light on their evolutionary dynamics and impact on genome innovation.

Results

Exceptional density of NUMTs and NUPTs in *T. gondii*

To identify insertions of organellar DNA fragments in the nuclear genome of *T. gondii* ME49 we applied the homology-based program Repeat Masker with organellar genomes as libraries. Only the 14 nuclear chromosomal assemblies and not all available contigs were queried for organellar insertions to obtain reliable and conservative estimates. The 21 conserved mtDNA sequence blocks (36) as well as full-length sequences of the mitochondrial protein-coding genes, *coxI*, *coxIII* and *cob* were included in the repeat library to minimize overestimation of the number of NUMTs. The 35 kb apicoplast genome sequence of *T. gondii* was utilized as the repeat library to identify NUPTs. These analyses revealed that 1.43% (895,312 bp) and 0.18% (112,433 bp) of the nuclear genome of *T. gondii* MR49 is composed of NUMTs and NUPTs respectively (Table 1, Fig. 1B, Dataset S1). To our knowledge, this percentage of nuclear genome occupied by NUOTs represents

163 the largest ever reported for any eukaryote (Table 1). Indeed, the NUMT insertions in *T. gondii* are
164 almost 6 times higher than the current overall record holder, the pathogenic fungus *Ustilago maydis*
165 (0.286%) (41) (Table 1).
166 Most (>90%) of the NUOTs identified in *T. gondii* are 50-200 bp in length and display <90%
167 sequence identity to their respective organellar DNA counterparts indicating most insertions have
168 accumulated mutations after nuclear acquisition (Fig. 1C). The largest NUMT is a single 3,369 bp
169 sequence on Chr 10 that does not contain any complete coding sequences but retains 99%
170 nucleotide identity to mtDNA sequence blocks suggesting it is a recent insertion (Table S1).
171 NUMTs derive from all 21 mtDNA SBs including coding and non-coding regions (Table S2).
172 Sequence blocks M, E, V and K are the most enriched each comprising at least 0.1 % of the nuclear
173 genome (Table S2). Similarly, NUPTs arise from nearly all regions of the apicoplast genome, with
174 the region between coordinates 9600 to 12000 being the least represented region in NUPTs
175 (Dataset S1).
176 We next examined the location and distribution of NUOTs in the *T. gondii* nuclear genome.
177 Approximately 60% of the identified NUOTs map to genic regions (introns and exons) with the vast
178 majority located in introns and the rest almost exclusively in UTRs (Table S3). The other 40% of
179 NUOTs are located in intergenic regions, and ~23% occur within the 1 kb flanking region of genes.
180 Thus, ~85% of *T. gondii* NUOTs reside within or near genes. This distribution is not unexpected
181 given the highly compact nature of the *T. gondii* genome where genes occupy ~70% of the nuclear
182 sequence.
183 To determine if NUOTs arose due to independent insertion events or were segmentally
184 duplicated post-insertion, we examined the flanking regions of NUOTs as duplication would likely
185 involve flanking nuclear sequence. We considered NUOTs to be the product of a nuclear segmental
186 duplication event if the NUOT along with 100 bp of its flanking regions was detected more than
187 once. Using this criterion, 105 NUMTs and 13 NUPTs were identified as segmentally duplicated
188 two to ten times in the ME49 nuclear genome sequence (Table S4). Since <1% of the NUOTs
189 were duplicated post-insertion suggesting, most NUOTs were independent insertion events.
190 Together, these findings demonstrate that the large proportion of NUOTs observed in the nuclear
191 genome of *T. gondii* arose primarily through independent insertion events that are generally <200
192 bp in length and display varying levels of sequence degeneration relative to their organellar DNA
193 counterparts.
194
195 **Strain-specific NUMTs indicate recent insertions and frequent turnover**
196 To determine the age distribution of the NUOTs, age-related decay was determined using $T = K/2\mu$
197 where μ is the intron mutation rate for *T. gondii* (10) and K, the genetic distance, was determined
198 with the Jukes-Cantor model based on the difference between the NUOT and organellar sequences
199 (see Methods). This analysis revealed a continuous influx of NUOT assimilations with a NUMT
200 accumulation peak approximately 7 million years ago (Fig. 1D). While NUOT assimilation appears
201 to be a continual process, most insertions occurred prior to the last 1 million years. The presence
202 of the NUOTs that are 100% identical to organellar DNA indicate that the process is ongoing.
203 To identify recent insertions or deletions we compared NUMTs in the nuclear genome of
204 different *T. gondii* strains. We restricted this investigation to NUMTs, since the number of NUMTs
205 is higher than NUPTs. We compared the NUMTs identified in *T. gondii* ME49 to those identified in
206 strains, GT1 and VEG, both of which have chromosomal level nuclear genome assemblies. We
207 identified a total of 32 strain-specific NUMTs: 12 in ME49, 13 in GT1 and 7 in VEG (Table S5). A
208 few of these strain-specific NUMTs were experimentally verified via PCR (Fig. S1, Table S6). 26 of
209 the 32 strain-specific NUMTs were found in or near annotated genes, suggesting that their
210 presence may have the potential to affect host gene activity (Table S5).
211 To ascertain if the strain-specific NUMTs arose via either a novel insertion or deletion
212 event, we determined sequence boundaries and performed a three-way genome comparison of
213 the regions in question. A NUMT was considered a novel insertion if it was precisely missing from
214 two of the three strains and displayed high sequence identity (>95%) when compared to the mtDNA
215 sequence (Fig. 2A). If a NUMT was missing in only one of the three strains and the NUMT in the
216 2 strains displayed high sequence divergence (>10%) when compared to the mtDNA, then we
217 concluded that this NUMT was most likely deleted in the third strain (Fig. 2B). Using such criteria,
218 3 NUMTs were confidently identified as novel insertions, and 13 were inferred to be deletions and

219 many of these are partial deletions (Table S5). These results suggest that NUMTs are dynamic and
220 can lead to strain differences in *Toxoplasma*.
221 To further explore the differential presence or absence of NUMTs in *T. gondii* we examined
222 13 additional strains with assembled, but less complete genome sequences. All of the strains
223 displayed a similar NUMT content (Table S7). Overall, we identified 8,271 ancestral NUMTs that
224 are present in all 16 strains and 56 NUMTs that show differential presence or absence among these
225 strains (Fig. 2C, Table S7). These differentially present NUMTs are in varying states of decay,
226 ranging from 0%-31% divergence from the mtDNA sequence. No strain shows a preferential loss
227 or gain/retention of NUMTs. MAS has the largest number of differential NUMTs at 36 out of 56 and
228 VEG the fewest (25/56) (Table S8).
229 The sites of insertion or deletion for the 56 differentially present NUMTs are mostly
230 conserved among the strains. Thus, it is likely that these NUMTs were inserted in an ancestor and
231 strains which evolved from this ancestor inherited the NUMT. For example, NUMTs 18 and 42
232 (100% identical to the mtDNA) are present only in strains MAS and TgCATBr5 and these strains
233 are clustered in Clade B (Fig. 2C) (7). NUMTs also appear to be inherited via recombination with
234 a strain that does not contain a given NUMT. For example, NUMTs 13, 35 and 37 that display 100%
235 identity to the mtDNA are each present in only two strains (p89 and VAND, TgCtCo5 and VAND
236 and GAB2-2007 and ME49 respectively) suggesting inheritance of the NUMT via recombination,
237 or, less likely, independent insertion of the same NUMT at the same location in different strains.
238 These pairs of strains are not members of the same clade and other clade members do not contain
239 these NUMTs (Fig. 2C). Genome analysis of *T. gondii* has demonstrated that the parasites undergo
240 sexual recombination at a higher frequency than previously thought (7). Our finding that NUMT
241 presence or absence does not follow clades is consistent with this observation.
242 Finally, to examine potential functional consequences of the 56 differentially present
243 NUMTs across the 16 *T. gondii* strains, we identified their insertion location with respect to genes.
244 8 are located in exons and 31 are located in introns. 11 NUMTs are located in flanking regions or
245 UTR, the remaining 6 are in intergenic regions outside of the 1 kb upstream and downstream
246 flanking regions (Table S8). None are located in a protein coding region. We conducted a gene-
247 ontology (GO) enrichment analysis with the 50 genes whose exons, introns or flanking regions
248 contained NUMTs. Genes involved in microtubule-based processes and movement (10 genes) and
249 nucleotide metabolic or biosynthetic processes (10 genes) are enriched 5-20 fold (Table S9).
250 These pathways and processes are core survival and virulence pathways as *T. gondii* acquires
251 purines from its host via salvage rather than *de novo* synthesis (42). It is possible that NUMTs in
252 these regions may affect transcription at these loci. However, transcriptome data are only available
253 for 3/16 strains analyzed here and only for tachyzoites.
254
255 **NUOTs are drivers of genome evolution in coccidian parasites**
256 To determine if the high NUOT density is a phenomenon specific to *T. gondii*, we investigated the
257 nuclear genome sequences of its closest coccidian relatives *Hammondia hammondi* and *Neospora*
258 *caninum* (Fig. 1A). *H. hammondi* contains NUMT and NUPT densities of 1.48% and 0.19%
259 respectively, a level higher than that observed in *T. gondii*. However, because the *H. hammondi*
260 genome sequence assembly is highly fragmented the NUOT densities are only estimates. The
261 NUOT content in *N. caninum's* nuclear genome is substantially lower than *T. gondii* at 0.66% for
262 NUMTs and 0.06% for NUPTs, however, these densities are still higher than those observed in
263 other eukaryotes (Table 1). By contrast, the distantly related coccidian species, *Sarcocystis*
264 *neurona* and *Eimeria tenella* display greatly reduced NUMT densities at 0.03 and 0.04%
265 respectively, relative to *T. gondii* and *N. caninum* but their NUPT densities, especially in the case
266 of *E. tenella*, are only slightly reduced relative to *T. gondii* (Table 1). Examination of the
267 apicomplexan nuclear genome sequences of species outside of the Coccidia revealed a paucity of
268 NUOTs. *Plasmodium falciparum* 3D7 contains only five NUMTs whereas we were unable to detect
269 any such insertions in *Babesia bovis* and *Theliera parva* (Table 1). Thus, an unusually high NUOT
270 density is a feature of coccidian parasites and is more pronounced in species closely related to *T.*
271 *gondii*.
272 Next, we examined the characteristics of the NUOTs in *N. caninum* and *H. hammondi*.
273 Similar to *T. gondii*, we found that most NUMTs are 50-200 bp in length in both species (Figs. S2 ,
274 S3). Greater than 90% of the NUOTs display less than 80% identity to the mt/ptDNA in *H.*

275 *hammondi* as is seen in *T. gondii*. Interestingly, the NUOTs in *N. caninum* appear younger (Fig. 1D
276 Figs. S2, S3) suggesting either more recent insertions, a different mutation rate or a more rapid
277 turnover rate in this species. NUPT's in *H. hammondi*, unlike the other coccidian species show two
278 distinct age populations, one quite recent (Fig. S3) but this may be an artifact related to
279 contaminating apicoplast sequences in the genome assembly. These results reveal that the
280 species most closely related to *T. gondii*, also have a very high NUOT density but that as you move
281 to more distant coccidian species, NUOTs decrease. In apicomplexans outside of the coccidia,
282 NOUTs are mostly non-existent.
283 Since NUMTs display an overall rapid turnover and decay based on comparisons between
284 *T. gondii* and *N. caninum* and within *T. gondii* strains, we hypothesized that evolutionary conserved
285 NUMTs might be under functional constraint, indicating cooption for cellular function. To identify
286 such coopted candidates, we compared the NUMTs between *T. gondii* and *N. caninum*, two
287 species that diverged ~28 MYA (43), and identified five orthologous NUMTs (Table S10). The
288 orthologous NUMT residing in the upstream region of the U6 snRNA-associated Sm family protein
289 encoding gene (TGME49_286560) was the most conserved NUMT, thus we selected this NUMT,
290 named NUMT[Sm]. NUMT[Sm] is 28.8% divergent from mtDNA SB U which encodes portions of
291 LSU and SSU rRNA fragments. Next we selected a younger *T. gondii* specific NUMT, called
292 NUMT[Myo] located in the upstream region of a putative myosin heavy chain gene
293 (TGME49_254850) of all examined *T. gondii* strains. NUMT[Myo] is 16.7% divergent from mtDNA
294 SB F which encodes RNA 10 (Fig. S3)(36). The upstream regions of both genes show evidence of
295 active transcription in *T. gondii* based on H3K9ac acetylation and H3K4 tri-methylation marks,
296 ToxoDB.org (44)(Fig. S4). The upstream regions of both *T. gondii* genes were cloned and tested
297 for their ability to drive luciferase gene expression in transient *in vitro* reporter assays in *T. gondii*
298 cultured parasites. For each promoter we generated luciferase reporter constructs where the
299 upstream region was wild-type or with the identified NUMT removed (Fig. 3A, B). Deletion of the
300 70 bp NUMT[Sm] significantly decreased promoter activity whereas deletion of the 66 bp
301 NUMT[Myo] dramatically increased promoter activity (Fig. 3C, D). These results suggest that
302 NUMTs can carry, or can evolve into cis-regulatory elements capable of modulating gene
303 expression. Taken together, these data demonstrate that NUMTs undergo rapid turnover and that
304 evolutionarily conserved insertions may have been retained due to functional constraints for
305 regulatory function.
306
307 **NUOT acquisition involves non-homologous end joining repair**
308 It has been demonstrated that organellar DNA fragments can become integrated into the nuclear
309 genome during the process of double-strand break (DSB) repair via a mechanism called non-
310 homologous end joining (NHEJ) (19, 20). NHEJ can repair DSBs without a template or sequence
311 homology but it often results in small deletions and in some cases insertion of short DNA sequences
312 (45). This mechanism of integration of DNA fragments, usually NUOTs but also transposable
313 elements was first demonstrated in *Saccharomyces cerevisiae* and subsequently proven in
314 mammalian cells and plants (19, 20, 46, 47). In *T. gondii*, it has been observed that DNA is readily
315 integrated into the nuclear genome at random sites via NHEJ (48). Indeed, it was necessary to
316 knock-out the gene encoding a critical NHEJ protein, Ku80, in order to increase the efficiency of
317 homologous recombination in this species (48). Interestingly, apicomplexans that lack the NHEJ
318 machinery also contain very few NUOTs (Fig. 4A, Table 1), suggesting that NHEJ is a prominent
319 mechanism underlying NUOT integration in coccidian species.
320 To experimentally test if NHEJ drives NUOT integration we used the CRISPR-Cas9 system
321 to generate targeted DSBs in the genome of a *T. gondii* RH wildtype strain as well as a *ku80* knock-
322 out mutant strain, Δ*ku80* (49, 50). We chose the *uprt* locus as the target for the DSB since disruption
323 of this gene leads to 5-fluorodeoxyribose (FUDR) resistance thus facilitating efficient selection for
324 improper repair of a CRISPR-Cas9 guide-directed cut (49). Resistant parasites were recovered,
325 DNA was extracted, the *uprt* locus was amplified and the amplicons were deep-sequenced using
326 Illumina paired-end sequencing (Table S11). Processed reads were then analyzed to compare the
327 number of insertions between wildtype and Δ*ku80* parasites and specifically for insertions of extra-

chromosomal DNA, including NUOTs and CRISPR-Cas9 plasmid DNA. It should be noted that nuclear DNA was also observed to be inserted at the DSB site but was not further investigated.

Overall, we observed that the number of unique reads obtained from WT parasites was seven times higher than that obtained from the Δ*ku80* strain (Table S11). Less than 1% of the reads from the Δ*ku80* parasites contained inserts of extrachromosomal DNA, whereas such insertions were observed in ~58% of the amplicons from wildtype *T. gondii* (Fig. 4B). Analysis of the source of DNA inserted at the DSB site revealed the transfected CRISPR-Cas9 plasmid was by far the most common source of inserted extra-chromosomal DNA both in terms of number of reads and number of base pairs inserted (Fig. 4B, C). We expected the majority of the inserts to be from plasmid DNA since it is readily available for repair following transfection. However, both mtDNA and ptDNA sequences were recovered as well, but surprisingly ptDNA insertions were slightly more common than mtDNA. This finding is in contrast to the observed higher levels of NUMTs versus NUPTs in the nuclear chromosomes of tissue coccidia (Table 1). Importantly, DNA capture was drastically reduced in the Δ*ku80* strain with no organellar DNA recovered at the DSB repair site (Fig. 4B, C).

We next compared insert length. Since only 150 bp from each end of the amplicon was sequenced, this analysis is limited to detecting a maximum insert length of ~250 bp. We observed that a large proportion of inserts from mtDNA were shorter (~110 bp) than those from ptDNA and plasmid DNA with the latter being the longest (Fig. 4 D, E). Inserts as long as 250 bp are detected from all three DNA sources. As is typically seen in NHEJ mediated repair, we detected insertion or deletion of a few base pairs at the repair site. We also observed simple insertions of one continuous stretch of DNA and a number of complex insertions where non-contiguous stretches of DNA from the same or multiple DNA sources were observed (Fig. 4F, Table S12). The insertions derived from all parts of the mt, pt or plasmid DNA and are of varying lengths (Table S12). These data indicate that DSB repair via NHEJ is the likely mechanism underlying NUOT integration in *T. gondii.* The properties of the observed insertions in an artificially induced DSB are similar to those observed in naturally acquired NUOTs with the exception that NUPTs were observed more often than NUMTs.

Discussion

DNA of organellar origin,NUOTs, can also be an important source of genetic variation. For example, a recent study of NUMTs in 66,038 human genome sequences revealed a complex and dynamic landscape with *de novo* NUMTs appearing in the germline once in every 10^4 births and somatic insertions once in every 10^3 cancer cells highlighting the ongoing formation and mutagenic potential of NUMTs in our species (16).

Our study shows that in the *Toxoplasmatinae*, which lack mobile elements, NUOTs are remarkably common and have been an important force in generating variation and evolution. To our knowledge, the *T. gondii* nuclear genome harbors the highest density of NUOTs ever reported at 1.61%. This percentage is more than 5-fold higher than the previous record holders *Arabidopsis thaliana* (0.25%) and *Ustilago maydis* (0.28%) (41).

The majority of the NUOTs in *T. gondii* arose from independent insertions rather than segmental duplications of previous insertions (51). However, unlike humans where NUMT insertions are concentrated in pericentromeric and subtelomeric regions (52). NUOTs in *T. gondii* and *N. caninum* occur evenly throughout the chromosome. A previous study reporting the presence of NUMTs in *T. gondii* found inverted repeats flanking the insertions (40). We have determined that the inverted repeat sequences are derived from mtDNA sequence block J, which is part of the *coxIII* gene. In our systematic catalog of 9379 NUMTs in the *T. gondii* genome, we rarely see inverted repeats flanking the NUMTs and SB J does not make up a higher proportion of the observed NUMT sequence, suggesting it is unlikely to be involved in propagating the NUMTs as had been suggested. The mtDNA of *T. gondii* is full of redundant sequence blocks often in alternative orientations within the same molecule (36). It should be noted that the high level of NUMTs in the nuclear genome, especially those with high similarity to the mtDNA was a significant confounding factor for the elucidation of the bizarre mtDNAs of *T. gondii*, *H. hammondi* and *N. caninum* as they made it impossible to use nucleic acid hybridization, PCR and genome assembly software (36).

Molecular and bioinformatic studies performed in yeast, tobacco and human have shown that integration of organellar DNA fragments occur during illegitimate repair of double-strand breaks

384 (DSBR) by non-homologous end joining (NHEJ) (22, 45, 53). We and others (54) do not find
385 homologs for the NHEJ proteins, KU70, KU80 and DNA ligase IV in *P. falciparum* and *T. parva* and
386 *B. bovis* only contains DNA ligase IV. Indeed, these organisms are known to predominantly employ
387 homologous recombination for DNA repair (21). The NHEJ proteins are present in *T. gondii* and
388 the other coccidians and we have validated their role in NUOT insertion in *T. gondii* by examining
389 repair of a CRISPR induced DSB in a Δ*ku80* strain. This strain was created because *T. gondii*
390 prefers NHEJ over other methods for DSB repair (48). The phylogenetic profile of the NHEJ
391 pathway genes and the fact that *T. gondii* uses NHEJ preferentially suggests that the proficiency
392 of the NHEJ pathway is sufficient to explain the high NUOT content in *T. gondii*. However, it doesn't
393 explain the variation in insertion levels observed between coccidian species.
394 We have shown that the NUMT content even within closely related apicomplexan species
395 varies significantly. These data are largely consistent with previous observations where a large
396 variation in NUMT content has been described among *Drosophila melanogaster*, *Anopheles*
397 *gambiae*, and *A. mellifera*, and even among mammals like human, mouse and rat (16, 17, 41, 55-
398 57). This variation may be explained by two major forces: differences in the frequency at which
399 species acquire and retain DNA from their mitochondria and the differential rates of NUMT removal
400 (56, 58). The frequency at which mtDNA is transferred to the nucleus can be influenced by many
401 factors, including the total number of mitochondria within a given cell, and the level of vulnerability
402 to stressful agents that may damage the mitochondria thereby releasing mtDNA. However, given
403 that apicomplexans generally contain only one mitochondrion (and apicoplast) per cell, this cannot
404 sufficiently explain the observable differences in NUMT (and NUPT) accumulation (59). There is
405 one significant difference between *Eimeria* and *Sarcocystis* which have fewer NUOTs and the high
406 NUOT group of *T. gondii, H. hammondi* and *N. caninum,* the former species contain transposable
407 elements (29, 60) whereas the others do not. Perhaps *Sarcocystis* and *Eimeria* have evolved
408 mechanisms for keeping the insertion of DNA under control and the *Toxoplasmatinae* lost this
409 ability when they cleared mobile elements from their genome. Alternatively, *the Toxoplasmatinae*
410 may benefit from this high level of genome variation precisely because they have lost their mobile
411 elements and the sources of genetic variation they provide. *Toxoplasma* in particular, also has the
412 added biology of being able to propagate asexually. This means it can spend long periods of time
413 as a haploid organism without a homologous chromosome to use as a repair template, which could
414 create additional advantages to having a steady supply of organellar DNA patches. There are
415 many hypotheses that deserve exploration.
416 A major unanswered question is how organellar DNA enters the nucleus and is available
417 for NHEJ repair. Analysis of existing NUOTs suggests that smaller fragments (100-200 bp) are
418 most frequently observed, but that significantly longer inserts are occasionally seen. NUMT inserts
419 appear to be random genome segments and do not correspond to the unique SBs of the *T. gondii*
420 mtDNA. It is possible that oxidative stress in the mitochondria may play a role in the generation of
421 random mtDNA fragments as single and double strand mtDNA breaks are observed in yeast (61-
422 63). But this explanation will not work for ptDNA fragments. The CRISPR DSB repair experiment
423 revealed slight differences in the insert lengths depending on insert DNA source with CRISPR
424 plasmid DNA inserts being longer than ptDNA which were slightly longer than mtDNA inserts. In
425 this experimental setting, NUPTs were also observed slightly more frequently than NUMTs a finding
426 that is at odds with the much higher abundance of NUMTs in *T. gondii* and all the other coccidian
427 genomes. The reason(s) why NUMTs greatly exceed NUPTs is unclear but likely reflects cell
428 biological differences in these independently acquired organelles. There are observed differences
429 in the calculated ages of NUOTs in the *Toxoplasmatinae* suggesting that different lineages have
430 experienced different waves of insertion or variation in removal that could not be recapitulated in
431 the experiments used here. We did observe the insertion of multiple non-continuous DNA
432 fragments including DNA from different sources both at the induced CRISPR DSB and naturally
433 occurring in the genome sequence attesting to the efficiency of DSB repair in *T. gondii*. These
434 mosaic inserts, termed NUMINs have been observed previously in plants (64).
435 Our attempt to identify NUOTs that were not ubiquitous in the 16 *T. gondii* strains examined
436 revealed 50 insertions in or near genes that were enriched in a Gene Ontology analysis for
437 processes related to microtubules and nucleotides. The distribution of NUMTs among the strains
438 revealed both recent insertion and patterns that are most easily explained as the result of sexual
439 recombination. Our search for orthologous NUOTs between *T. gondii* and *N. caninum* resulted in

only 5 orthologous NUMTs and no orthologous NUPTs. This finding highlights the efficiency with which NUOTs are removed from the genome. These species diverged an estimated 28 MY ago (43). Of the 5 detectable NUMTs, one was more conserved relative to surrounding sequence, suggesting it may have evolved under functional constraint and might shed light on the types of evolutionary innovation NUOTs can provide. Indeed, functional assays suggest it might act as a cis-regulatory element affecting promoter activity of the U6 snRNA associated Sm family protein as promoter activity was reduced upon NUMT removal in a reporter construct. All coccidians have a large number of introns thus, one could speculate that this might confer an effect, but this would need to be tested. Surprisingly, the *T. gondii*-specific NUMT which is inserted near the putative myosin heavy chain ATPase gene in all strains examined dramatically decreases the gene promoter activity. These findings are intriguing because they suggest that both ancient and recent NUMT insertions can influence gene regulation. Because the putative myosin heavy chain ATPase gene implicated here belongs to a diverse family of proteins involved in parasite motility, division and penetration of host cells (65), it is possible that the NUMT inserted within its promoter region, could modulate the pathogenicity and virulence of the parasite, but this remains to be proven. NUMTs are increasingly associated with functional consequences, particularly in human diseases (52) and mitigating deletions in the evolution of primates (45). For example, mtDNA instability and increased NUMT somatic integration has been associated with colorectal adenocarcinoma (66).

Conclusion

Following identification of both *T. gondii* organellar genome sequences, it became possible to characterize the NUMTs and NUPTs that have hindered some molecular studies of these organellar DNAs. Shockingly, this protist pathogen and its closest relatives *H. hammondi* and *N. caninum* harbor the highest NUOT density ever observed. While most NUOTs exhibit various levels of sequence decay, several inserts are identical in sequence to their organellar source suggesting they are recent and that nuclear insertion and turnover of organellar DNA is an ongoing process in these species. NHEJ was shown to be essential for repair of an induced DSB. Examination of 16 *T. gondii* strains revealed 56 insertions that are differentially present and a search for orthologous insertions in *N. caninum* yielded 5 NUMTs. Deletion of one orthologous and one non-orthologous NUMT affected gene expression of reporter constructs. To our knowledge this is the first study to experimentally establish that NUMTs can also influence gene expression. NUOTs provide a previously unexplored source of genomic variation in these important pathogens.

Materials and Methods

Source of genome Sequences.

The nuclear genomic sequences of *Toxoplasma gondi* ME49 (NCBI assembly GCA_000006565.1), *Hammondia hammondi* H.H.34 (GCA_000258005.1) *Neospora caninum* Liverpool (GCA_000208865.1), *Sarcocystis neurona* SN3 (GCA_000727475.1), *and Eimeria tenella* Houghton (GCA_000499545.1) were downloaded from ToxoDB.org (44). *Plasmodium falciparum* 3D7 (GCA_000002765.1), *Babesia bovis* (GCA_000165395.1) and *Theileria annulata* (GCA_000003225.1) nuclear as well as organellar genome sequences were obtained from PlasmoDB.org and PiroplasmaDB.org respectively.

Identification of NUMTs and NUPTs.

RepeatMasker version 4.0.5 (http://www.repeatmasker.org) was used to identify organellar DNA sequences in the nuclear genome sequences. mtDNA and ptDNA seqeunces were used as the "repeat library" and "cross_match" was used with filtering out low complexity sequences and other parameters as default, to mask the corresponding nuclear genomes to identify NUMTs and NUPTs respectively. For *T. gondii* and *N. caninum* the species-specific 21 sequence blocks as well as cytochrome coding sequences, *coxI*, *coxIII* and *cob* (36) were used to mask the nuclear chromosomal sequences. *T. gondii* apicoplast sequence (GenBank: U87145.2) was used to detect NUPTs in *T. gondii* ME49 and *N. caninum* Liverpool. *T. gondii* mtDNA and ptDNA sequences were used to identify NUOTs in *H. hammondi*. The partial cytochrome sequences annotated in *S. neurona* and *T. gondii* mtDNA sequences were used to identify NUMTs in *S. neurona* and the *S.*

496 *neurona* ptDNA sequence was used to identify NUPTs. NUMTs and NUPTs in *E. tenella* were
497 detected using its own organellar sequences (GenBank Accessions: AB564272.1 and
498 AY217738.1. Similarly, *Plasmodium, Babesia* and *Theileria* species-specific organellar sequences
499 obtained from VEuPathDB.org were used to screen their respective nuclear chromosome
500 sequences for NUOTs and genes involved in the NHEJ DSB repair pathway. NUOTs shorter than
501 28 bp and overlapping insertions were only counted once.
502
503 **Identification of NUMT location**
504 Coordinates of coding regions, introns, exons, intergenic and 1 kb upstream and downstream
505 flanking regions were obtained from the annotation data available on ToxoDB.org release 13 (44).
506 Based on coordinates, a custom script was used to identify the genomic location for each NUMT.
507 NUMTs located in non-coding exons were classified as being present in the UTR. NUMTs spanning
508 more than one genomic feature were classified separately. Insertion sites were inspected to see if
509 a target site preference could be observed.
510
511 **Identification of segmental duplications, shared and uniquely-present NUMTs**
512 Segmental duplications were identified by extracting NUMT sequences along with 150 bp of the
513 flanking regions. The extracted sequences were used as BLASTN queries against themselves. If
514 a NUMT along with at least 100bp of flanking sequence was present at least twice it was counted
515 as a segmental duplication (27). Following the identification NUMTs in *T. gondii* ME49 reference
516 nuclear genome, NUMTs were similarly identified in nuclear genomes of the fully assembled *T.*
517 *gondii* strains, GT1 and VEG and *de novo* assembled sequences of ARI, CAST, TgCtBr5, TgCtBr9,
518 TgCtPRC2, COUG, TgCtCo5, FOU, GAB2-2007-GAL-DOM2, MAS, p89, RUB and VAND,
519 obtained from ToxoDB.org (44). Any scaffold or contig that contained only mtDNA sequence was
520 excluded. In order to identify NUMTs that were shared or unique to a strain, each NUMT sequence
521 along with 200 bp of flanking sequences was searched against the NUMTs with 200 bp flanking
522 sequences of all other strains using BLASTN. NUMTs that were present in only one strain were
523 called strain-specific *T. gondii* NUMTs. NUMTs that are present in all are called 'shared'. Strain-
524 specific NUMTs in ME49, GT1 and VEG were manually verified. A similar approach was utilized to
525 identify NUMTs that were shared or uniquely present among *T. gondii* ME49 and *N. caninum*. All
526 BLASTN search results were filtered for an E-value = 0 and query coverage of >90%.
527
528 **Estimation of NUOT age**
529 The relative date of insertion of a NUMT can be inferred from the NUMTs age. RepeatMasker
530 reports a percent divergence between the NUMT and the corresponding mtDNA sequence. The
531 percent divergences were converted into genetic distances using the Jukes-Cantor Model formula
532 $K = -\frac{3}{4}\ln(1-\frac{4}{3}p)$, where K is the genetic distance and p is the percent divergence between
533 the mtDNA and NUMT. Percent divergence was calculated by dividing the number of substitutions
534 between the two sequences by the sequence length. Using the genetic distance the age of each
535 NUMT was calculated using the formula, $T = K/2\mu$, where T is the age of the NUMT, K is the genetic
536 distance (Dataset S1), μ is the intron mutation rate. The intron mutation rate was used to calculate
537 the age of the NUMTs since NUMTs are not expected to be under selective pressure and should
538 have a neutral mutation rate similar to the introns. The intron mutation rate was previously
539 calculated as 2.12×10^{-8} (10). The same rate was for used for all three species.
540
541 **Expression constructs and Transient Transfection**.
542 PCR primers (Table S6) containing the attB1 and attB2 sites were used to amplify the appropriate
543 promoter and 5′-UTR regions from ME49 genomic DNA for the two genes tested. A two-step
544 overlap-extension PCR technique (67) was employed to delete the NUMT from each promoter.
545 Following sequencing verification, these promoter fragments were moved into a Firefly luciferase-
546 expressing vector. As constitutive *T. gondii* promoter (α-tubulin)-driven Renilla luciferase-
547 expressing construct was co-transfected along with the experimental construct. Parasite culture
548 and transient transfections were performed as described (68). A dual luciferase assay was
549 performed on the extract using the Promega Dual Luciferase kit. Reporter activity from the WT or
550 ΔNUMT promoter was measured relative to the internal control. Each electroporation experiment

was performed 6 times and luciferase assays were performed in duplicate for expression measurements. The unpaired Students *t*-test was used to calculate the statistically significant difference in expression levels between WT and mutagenized promoter activity; $p < 0.05$ was considered statistically significant.

CRISPR-Cas9 transfection assays, amplicon sequencing and analysis of inserts

T. gondii strains RH and an RH mutant TATiΔ*ku80*, referred here as WT and Δ*ku80* (69) respectively were cultured on human immortalized fibroblast cells grown in Dulbecco's Modified Eagle's Medium supplemented with 10% heat-inactivated Cosmic Calf Serum, 0.5% 10mg/ml penicillin-streptomycin and 0.05% 10 mg/ml gentamycin. *T. gondii* RH WT and Δ*ku80* parasites were filtered, washed and resuspended in cytomix (supplemented with ATP and glutamine) at a concentration of 3.3×10^7 parasites/ml. 10^7 parasites were electroporated with 8 µg of the CRISPR/Cas9 plasmid with a single guide RNA targeting the UPRT locus utilizing a BTX electroporator. hTERT cells were infected with the transfected parasites (WT or Δ*ku80* in triplicate) and grown for 48 hr without drug selection. After 48 hr, lysed parasites were passed to fresh hTERT cells and placed under 10 µM of 5-fluorodeoxyuridine (5-FUDR) drug selection to select for parasites with a non-functional UPRT gene. Parasites were harvested following four rounds of drug selection and DNA was extracted using Qiagen Blood and Tissue kit. PCR amplicons of the UPRT locus from DNA extracted from all six transfections were generated. Amplicons were indexed and Illumina MiSeq PE-150 bp sequencing was performed. Filtered and trimmed paired-end reads were then merged using FLASH (default parameters) (70, 71). Unique reads were identified using the usearch fastx_uniques script (72). The unique reads were then investigated for the presence of *T. gondii* mtDNA (21 sequence blocks), ptDNA, and CRISPR/Cas9 plasmid DNA sequences using RepeatMasker and each genome sequence as a repeat library. RepeatMasker results were then analyzed to identify the characteristics of the inserts reported in Fig. 4.

Acknowledgments

We thank Drs. Michael Cipriano (University of Georgia) and Boris Striepen (University of Pennsylvania) for generously providing the RH mutant TATiΔ*ku80* and the CRISPR/Cas9 plasmid. This work was funded by NIH R01AI068908 to JCK.

Data sharing

Amplicon sequences are available via NCBI BioProject PRJNA961209.

References

1. A. M. Tenter, A. R. Heckeroth, L. M. Weiss, *Toxoplasma gondii*: from animals to humans. *Int J Parasitol* **30**, 1217-1258 (2000).
2. J. P. Dubey, *Toxoplasmosis of Animals and Humans* (CRC Press, ed. Third Edition, 2021).
3. F. Robert-Gangneux, M. L. Darde, Epidemiology of and diagnostic strategies for toxoplasmosis. *Clin Microbiol Rev* **25**, 264-296 (2012).
4. F. Belanger, F. Derouin, L. Grangeot-Keros, L. Meyer, Incidence and risk factors of toxoplasmosis in a cohort of human immunodeficiency virus-infected patients: 1988-1995. HEMOCO and SEROCO Study Groups. *Clinical infectious diseases : an official publication of the Infectious Diseases Society of America* **28**, 575-581 (1999).
5. R. E. Gilbert *et al.*, Effect of prenatal treatment on mother to child transmission of *Toxoplasma gondii:* retrospective cohort study of 554 mother-child pairs in Lyon, France. *Int J Epidemiol* **30**, 1303-1308 (2001).
6. C. Su *et al.*, Globally diverse *Toxoplasma gondii* isolates comprise six major clades originating from a small number of distinct ancestral lineages. *Proceedings of the National Academy of Sciences of the United States of America* **109**, 5844-5849 (2012).
7. H. Lorenzi *et al.*, Local admixture of amplified and diversified secreted pathogenesis determinants shapes mosaic *Toxoplasma gondii* genomes. *Nat Commun* **7**, 10147 (2016).
8. E. K. Shwab *et al.*, Geographical patterns of *Toxoplasma gondii* genetic diversity revealed by multilocus PCR-RFLP genotyping. *Parasitology* **141**, 453-461 (2014).

9. E. Bertranpetit *et al.*, Phylogeography of *Toxoplasma gondii* points to a South American origin. *Infect Genet Evol* **48**, 150-155 (2017).
10. C. Su *et al.*, *Recent exp*ansion of *Toxoplasma* through enhanced oral transmission. *Science* **299**, 414-416 (2003).
11. T. Kleine, U. G. Maier, D. Leister, DNA Transfer from Organelles to the Nucleus: The Idiosyncratic Genetics of Endosymbiosis. *Annual Review of Plant Biology* **60**, 115-138 (2009).
12. M. W. Gray, G. Burger, B. F. Lang, Mitochondrial evolution. *Science* **283**, 1476-1481 (1999).
13. J. L. Boore, Animal mitochondrial genomes. *Nucleic acids research* **27**, 1767-1780 (1999).
14. W. Martin *et al.*, Evolutionary analysis of *Arabidopsis*, cyanobacterial, and chloroplast genomes reveals plastid phylogeny and thousands of cyanobacterial genes in the nucleus. *Proceedings of the National Academy of Sciences of the United States of America* **99**, 12246-12251 (2002).
15. F. M. Calabrese *et al.*, NumtS colonization in mammalian genomes. *Sci Rep* **7**, 16357 (2017).
16. W. Wei *et al.*, Nuclear-embedded mitochondrial DNA sequences in 66,083 human genomes. *Nature* **611**, 105-114 (2022).
17. G. Dayama, W. Zhou, J. Prado-Martinez, T. Marques-Bonet, R. E. Mills, Characterization of nuclear mitochondrial insertions in the whole genomes of primates. *NAR Genom Bioinform* **2**, lqaa089 (2020).
18. M. Lang *et al.*, Polymorphic NumtS trace human population relationships. *Hum Genet* **131**, 757-771 (2012).
19. X. Yu, A. Gabriel, Patching broken chromosomes with extranuclear cellular DNA. *Mol Cell* **4**, 873-881 (1999).
20. M. Ricchetti, C. Fairhead, B. Dujon, Mitochondrial DNA repairs double-strand breaks in yeast chromosomes. *Nature* **402**, 96-100 (1999).
21. G. Barja, Updating the mitochondrial free radical theory of aging: an integrated view, key aspects, and confounding concepts. *Antioxid Redox Signal* **19**, 1420-1445 (2013).
22. K. Henze, W. Martin, How do mitochondrial genes get into the nucleus? *Trends Genet* **17**, 383-387 (2001).
23. J. Wasmuth, J. Daub, J. M. Peregrín-Alvarez, C. A. M. Finney, J. Parkinson, The origins of apicomplexan sequence innovation. *Genome Research* **19**, 1202-1213 (2009).
24. J. D. DeBarry, J. C. Kissinger, Jumbled genomes: missing Apicomplexan synteny. *Molecular biology and evolution* **28**, 2855-2871 (2011).
25. C. Feschotte, E. J. Pritham, DNA transposons and the evolution of eukaryotic genomes. *Annu Rev Genet* **41**, 331-368 (2007).
26. J. N. Wells, C. Feschotte, A Field Guide to Eukaryotic Transposable Elements. *Annu Rev Genet* **54**, 539-561 (2020).
27. A. B. Barrie (2010) Role of Repetitive DNA in Apicomplexan Genome Evolution. in *Biology* (University of Texas at Arlington), p 79.
28. T. J. Templeton *et al.*, A genome-sequence survey for *Ascogregarina taiwanensis* supports evolutionary affiliation but metabolic diversity between a Gregarine and *Cryptosporidium*. *Molecular biology and evolution* **27**, 235-248 (2010).
29. T. Blazejewski *et al.*, Systems-based analysis of the *Sarcocystis neurona* genome identifies pathways that contribute to a heteroxenous life cycle. *mBio* **6** (2015).
30. A. Seidi *et al.*, Elucidating the mitochondrial proteome of *Toxoplasma gondii* reveals the presence of a divergent cytochrome c oxidase. *Elife* **7** (2018).
31. D. S. Roos *et al.*, Origin, targeting, and function of the apicomplexan plastid. *Curr Opin Microbiol* **2**, 426-432 (1999).
32. N. Egea, N. Lang-Unnasch, Phylogeny of the large extrachromosomal DNA of organisms in the phylum Apicomplexa. *J Eukaryot Microbiol* **42**, 679-684 (1995).
33. R. J. Wilson, M. J. Gardner, J. E. Feagin, D. H. Williamson, Have malaria parasites three genomes? *Parasitol Today* **7**, 134-136 (1991).

662 34. G. I. McFadden, M. E. Reith, J. Munholland, N. Lang-Unnasch, Plastid in human
663 parasites. *Nature* **381**, 482 (1996).
664 35. R. F. Waller, G. I. McFadden, The apicoplast: a review of the derived plastid of
665 apicomplexan parasites. *Curr Issues Mol Biol* **7**, 57-79 (2005).
666 36. S. Namasivayam *et al.*, A novel fragmented mitochondrial genome in the protist pathogen
667 *Toxoplasma gondii* and related tissue coccidia. *Genome Res* **31**, 852-865 (2021).
668 37. L. Berna, N. Rego, M. E. Francia, The Elusive Mitochondrial Genomes of Apicomplexa:
669 Where Are We Now? *Front Microbiol* **12**, 751775 (2021).
670 38. C. J. Jackson, S. G. Gornik, R. F. Waller, The mitochondrial genome and transcriptome
671 of the basal dinoflagellate *Hematodinium* sp.: character evolution within the highly
672 derived mitochondrial genomes of dinoflagellates. *Genome Biol Evol* **4**, 59-72 (2012).
673 39. R. F. Waller, C. J. Jackson, Dinoflagellate mitochondrial genomes: stretching the rules of
674 molecular biology. *Bioessays* **31**, 237-245 (2009).
675 40. P. N. Ossorio, L. D. Sibley, J. C. Boothroyd, Mitochondrial-like DNA sequences flanked
676 by direct and inverted repeats in the nuclear genome of *Toxoplasma gondii*. *J Mol Biol*
677 **222**, 525-536 (1991).
678 41. E. Hazkani-Covo, R. M. Zeller, W. Martin, Molecular Poltergeists: Mitochondrial DNA
679 Copies (numts) in Sequenced Nuclear Genomes. *PLoS genetics* **6**, e1000834 (2010).
680 42. B. A. Fox, D. J. Bzik, *De novo* pyrimidine biosynthesis is required for virulence of
681 *Toxoplasma gondii. Nature* **415**, 926-929 (2002).
682 43. A. J. Reid *et al.*, Comparative genomics of the apicomplexan parasites *Toxoplasma*
683 *gondii* and *Neospora caninum*: Coccidia differing in host range and transmission strategy.
684 *PLoS pathogens* **8**, e1002567 (2012).
685 44. J. C. Kissinger, B. Gajria, L. Li, I. T. Paulsen, D. S. Roos, ToxoDB: accessing the
686 *Toxoplasma gondii* genome. *Nucleic acids research* **31**, 234-236 (2003).
687 45. E. Hazkani-Covo, S. Covo, Numt-mediated double-strand break repair mitigates deletions
688 during primate genome evolution. *PLoS genetics* **4**, e1000237 (2008).
689 46. Y. Lin, A. S. Waldman, Promiscuous patching of broken chromosomes in mammalian
690 cells with extrachromosomal DNA. *Nucleic acids research* **29**, 3975-3981 (2001).
691 47. Y. Lin, A. S. Waldman, Capture of DNA sequences at double-strand breaks in
692 mammalian chromosomes. *Genetics* **158**, 1665-1674 (2001).
693 48. B. A. Fox, J. G. Ristuccia, J. P. Gigley, D. J. Bzik, Efficient gene replacements in
694 *Toxoplasma gondii* strains deficient for nonhomologous end joining. *Eukaryot Cell* **8**, 520-
695 529 (2009).
696 49. B. Shen, K. M. Brown, T. D. Lee, L. D. Sibley, Efficient gene disruption in diverse strains
697 of *Toxoplasma gondii* using CRISPR/CAS9. *mBio* **5**, e01114-01114 (2014).
698 50. S. M. Sidik, C. G. Hackett, F. Tran, N. J. Westwood, S. Lourido, Efficient genome
699 engineering of *Toxoplasma gondii* using CRISPR/Cas9. *PloS one* **9**, e100450 (2014).
700 51. D. Bensasson, M. W. Feldman, D. A. Petrov, Rates of DNA duplication and mitochondrial
701 DNA insertion in the human genome. *Journal of molecular evolution* **57**, 343-354 (2003).
702 52. M. J. Puertas, M. Gonzalez-Sanchez, Insertions of mitochondrial DNA into the nucleus-
703 effects and role in cell evolution. *Genome* **63**, 365-374 (2020).
704 53. J. L. Blanchard, G. W. Schmidt, Mitochondrial DNA migration events in yeast and
705 humans: integration by a common end-joining mechanism and alternative perspectives
706 on nucleotide substitution patterns. *Molecular biology and evolution* **13**, 893 (1996).
707 54. A. Nenarokova *et al.*, Causes and Effects of Loss of Classical Nonhomologous End
708 Joining Pathway in Parasitic Eukaryotes. *mBio* **10** (2019).
709 55. P. Pamilo, L. Viljakainen, A. Vihavainen, Exceptionally high density of NUMTs in the
710 honeybee genome. *Molecular biology and evolution* **24**, 1340-1346 (2007).
711 56. E. Richly, D. Leister, NUMTs in sequenced eukaryotic genomes. *Molecular biology and*
712 *evolution* **21**, 1081-1084 (2004).
713 57. D. Bensasson, D. Zhang, D. L. Hartl, G. M. Hewitt, Mitochondrial pseudogenes:
714 evolution's misplaced witnesses. *Trends Ecol Evol* **16**, 314-321 (2001).
715 58. K. L. Adams, J. D. Palmer, Evolution of mitochondrial gene content: gene loss and
716 transfer to the nucleus. *Mol Phylogenet Evol* **29**, 380-395 (2003).

717 59. F. Seeber, J. Limenitakis, D. Soldati-Favre, Apicomplexan mitochondrial metabolism: a
718 story of gains, losses and retentions. *Trends Parasitol* **24**, 468-478 (2008).
719 60. M. Rodriguez, W. Makalowski, Mobilome of Apicomplexa Parasites. *Genes (Basel)* **13**
720 (2022).
721 61. P. M. Girard, S. Boiteux, Repair of oxidized DNA bases in the yeast *Saccharomyces*
722 *cerevisiae*. *Biochimie* **79**, 559-566 (1997).
723 62. N. A. Doudican, B. Song, G. S. Shadel, P. W. Doetsch, Oxidative DNA damage causes
724 mitochondrial genomic instability in *Saccharomyces cerevisiae*. *Mol Cell Biol* **25**, 5196-
725 5204 (2005).
726 63. P. E. Thorsness, E. R. Weber, Escape and migration of nucleic acids between
727 chloroplasts, mitochondria, and the nucleus. *Int Rev Cytol* **165**, 207-234 (1996).
728 64. S. Portugez, W. F. Martin, E. Hazkani-Covo, Mosaic mitochondrial-plastid insertions into
729 the nuclear genome show evidence of both non-homologous end joining and homologous
730 recombination. *BMC Evol Biol* **18**, 162 (2018).
731 65. M. Meissner, D. Schluter, D. Soldati, Role of *Toxoplasma gondii* myosin A in powering
732 parasite gliding and host cell invasion. *Science* **298**, 837-840 (2002).
733 66. V. Srinivasainagendra *et al.*, Migration of mitochondrial DNA in the nuclear genome of
734 colorectal adenocarcinoma. *Genome Med* **9**, 31 (2017).
735 67. J. Sambrook, E. R. Fritsch, T. Maniatis, *Molecular Cloning: A laboratory Manual* (Cold
736 Spring Harbor Laboratory Press, Cold spring Harbor, NY, ed. 2nd, 1989).
737 68. N. Mullapudi, S. J. Joseph, J. C. Kissinger, Identification and functional characterization
738 of cis-regulatory elements in the apicomplexan parasite *Toxoplasma gondii. Genome Biol*
739 **10**, R34 (2009).
740 69. L. Sheiner *et al.*, A systematic screen to discover and analyze apicoplast proteins
741 identifies a conserved and essential protein import factor. *PLoS pathogens* **7**, e1002392
742 (2011).
743 70. A. M. Bolger, M. Lohse, B. Usadel, Trimmomatic: a flexible trimmer for Illumina sequence
744 data. *Bioinformatics* **30**, 2114-2120 (2014).
745 71. T. Magoc, S. L. Salzberg, FLASH: fast length adjustment of short reads to improve
746 genome assemblies. *Bioinformatics* **27**, 2957-2963 (2011).
747 72. R. C. Edgar, B. J. Haas, J. C. Clemente, C. Quince, R. Knight, UCHIME improves
748 sensitivity and speed of chimera detection. *Bioinformatics* **27**, 2194-2200 (2011).
749
750

751 **Figure Legends**
752
753 **Figure 1. Characteristics of NUMTs and NUPTs in *T. gondii* ME49** *(A)* Cladogram of
754 apicomplexan parasite relationships *(B)* Circos plot (Circos version 0.51) represents the distribution
755 of NUMTs and NUPTs in the nuclear chromosomes of *T. gondii* ME49. The outer circle of yellow
756 bands indicates the chromosomes as labeled and each tick on the band equals 100 kb. The ticks
757 interior to the chromosomes are different features as indicated in the key. *(C)* The length and the
758 percent identity of a NUMT and NUPT to mt and ptDNA respectively was calculated from
759 RepeatMasker results and the distribution is plotted. *(D)* The age of each NUMT and NUPT was
760 calculated based on the percent divergence from the mt and ptDNA of the corresponding species
761 and the distribution of the age is plotted against the number of base pairs.
762
763 **Figure 2. Strain-specific presence and absence of NUMTs in *T. gondii*** *(A, B)* A likely strain-
764 specific insertion in *T. gondii* (TG) GT1 *(A)* and deletion in ME49 *(B)* are shown. A multiple
765 sequence alignment of these loci was performed for strains GT1, VEG and ME49 and the co-
766 ordinates of the loci are indicated with reference with GT1 chromosome VI. The NUMT and flanking
767 nuclear sequence are indicated in red and black respectively. *(C)* NUMTs in 16 *T. gondii* strains
768 were compared to identify a strain-specific presence and absence. Strains are grouped and colored
769 by clades as previously identified (7). The 14 chromosomes divided by black lines are represented
770 on the x-axis. NUMTs that show differential presence/absence in the 16 *T. gondii* strains are
771 numbered and ordered based on their location in ME49. The coordinates of each NUMT plus 200
772 bp flanking region on the ME49 chromosomes are shown at the bottom. The 200 bp regions were
773 included to provide a location for NUMTs missing in ME49. The percent divergence of the NUMT
774 from the mtDNA sequence is indicated above the coordinates. In the matrix, "+" and "-" indicate
775 presence and absence of a NUMT in a particular strain. Each cell is colored based on local clade
776 ancestry of that location (7) although, it does not imply that location originated from that clade.
777 Yellow cells indicate clade E ancestry and were not included the NUMT analysis as an assembled
778 genome sequence for a strain from this clade was not available
779
780
781 **Figure 3. Cis-regulatory activity of two selected NUMTs** *(A, B)* The structure of WT and NUMT
782 deletion promoter constructs for U6 snRNA-associated Sm family protein gene TGME49_286560
783 *(A)* and myosin heavy chain gene TGME49_254850 *(B)*. Nucleotide positions are referenced with
784 respect to the start of translation (+1) of host gene and the red region indicates the position of the
785 NUMT (Fig. S3). *(C, D)* Reporter assay results for the promoter of Sm-like protein *(C)* and mysoin
786 heavy chain *(D)* genes. The graphs depict luciferase activity as ratios of Firefly:Renilla activity in
787 relative luciferase units (RLU) from the different constructs containing either WT or mutagenized
788 promoter. All luciferase readings are relative to an internal control (α-tubulin-Renilla). Error bars
789 represent standard error calculated across the means of six independent electroporations. P-
790 values were calculated using Student's *t*-test.
791
792 **Figure 4. Capture of DNA insertions at CRISPR/Cas9-directed double-strand break at *uprt*
793 *locus* in wildtype and** Δ*ku80* parasites**.** Utilizing the CRISPR-Cas9 system, double-strand breaks
794 were induced at the *uprt* locus in wildtype *T. gondii* and Δ*ku80* parasites. The locus was then
795 amplified and deep-sequenced to evaluate the extrachromosomal DNA insertions (mtDNA, ptDNA,
796 CRISPR-Cas9 plasmid DNA) at the DSB site. *(A)* Apicomlexan cladogram with presence (+) or
797 absence (-) of key NHEJ pathway genes and NUOT content in each species indicated. The
798 coccidian branch is shown in bold. *(B, C)* The percent of amplicons with insertions from each DNA
799 type *(B)* and the percentage of base pairs from each type present in the amplicons *(C)* are plotted
800 for WT and Δ*ku80* parasites. The amplicons analyzed comprise all read pairs that could be merged
801 as well as unmerged reads. Error bars represent standard error of means of three replicates.
802 Statistical significance was calculated using Student's *t*-test (* $p < 0.05$, ** $p < 0.01$, *** $p < 0.001$).
803 *(D, E)* Distribution of the insert length for each DNA type is plotted as a proportion *(D)* and as box
804 plots *(E)*. The data were generated from merged read pairs for one WT replicate. Color key is as
805 shown in *(B)*. Statistical significance was calculated using Student's *t*-test (**** $p < 0.0001$). *(F)*
806 Schematic representation of the modifications observed in the amplicon reads for WT parasites.

807 The numbers under 'WT amplicon' indicate the length of the amplicon with the inverted triangle
808 denoting the approximate site of the double strand break. The type of DNA inserted is indicated in
809 the key in *(A)*. Not all combinations of insertion patterns observed in the reads are represented.
810 Examples of reads with the kind of modifications shown in this schematic are provided in Table
811 S12. Amplicons with WT sequence (yellow) on both ends represent reads where the pairs could
812 be merged. Numerous unmerged read with similar insertion patterns as shown in this figure exist
813 but are not drawn here.
814

815 **Table 1.** NUMTs and NUPTs detected in apicomplexan other eukaryotic genome sequences
816

Apicomplexan Species	NUMTs			NUPTs		
	Density (%)	Number of insertions	Number of base pairs	Density (%)	Number of insertions	Number of base pairs
T. gondii ME49[1]	1.430	9,379	895,312	0.180	1,108	112,443
H. hammondi H.H.34[1]	1.480	10,643	999,296	0.190	1,206	117,917
N. caninum LIV[1]	0.660	4,534	380,139	0.060	373	34,236
S. neurona SN3	0.030	454	38,353	0.020	54	27,624
E. tenella Houghton	0.040	227	22,024	0.088	338	45,513
B. bovis	0.000	0	0	0.020	11	1,697
T. parva	0.000	0	0	0.010	7	1,036
P. falciparum	0.002	5	515	0.020	30	5,408
Other Eukaryotes (41)						
A. thaliana	0.2564	820	305,602	0.03	301	50
O. sativa	0.1768	5,357	823,923	0.15	2090	782
H. sapiens	0.0087	871	263,478			
S. cerevisiae	0.0081	18	983			
D. melanogaster	0.0057	50	10,331			
M. musculus	0.0015	137	37,670			
C. elegans	0.0001	1	126			
M. domestica	0.0698	1859	2,093,630			
A. mellifera	0.0861	1,790	172,131			

817 [1]Non-contiguous DNA from organellar genomes can be inserted into the same locus during the
818 same insertion event. Therefore one caveat of the approach used is overestimation of the number
819 of insertion events. The identification of the amount of DNA inserted is not affected.
820

Figure 1

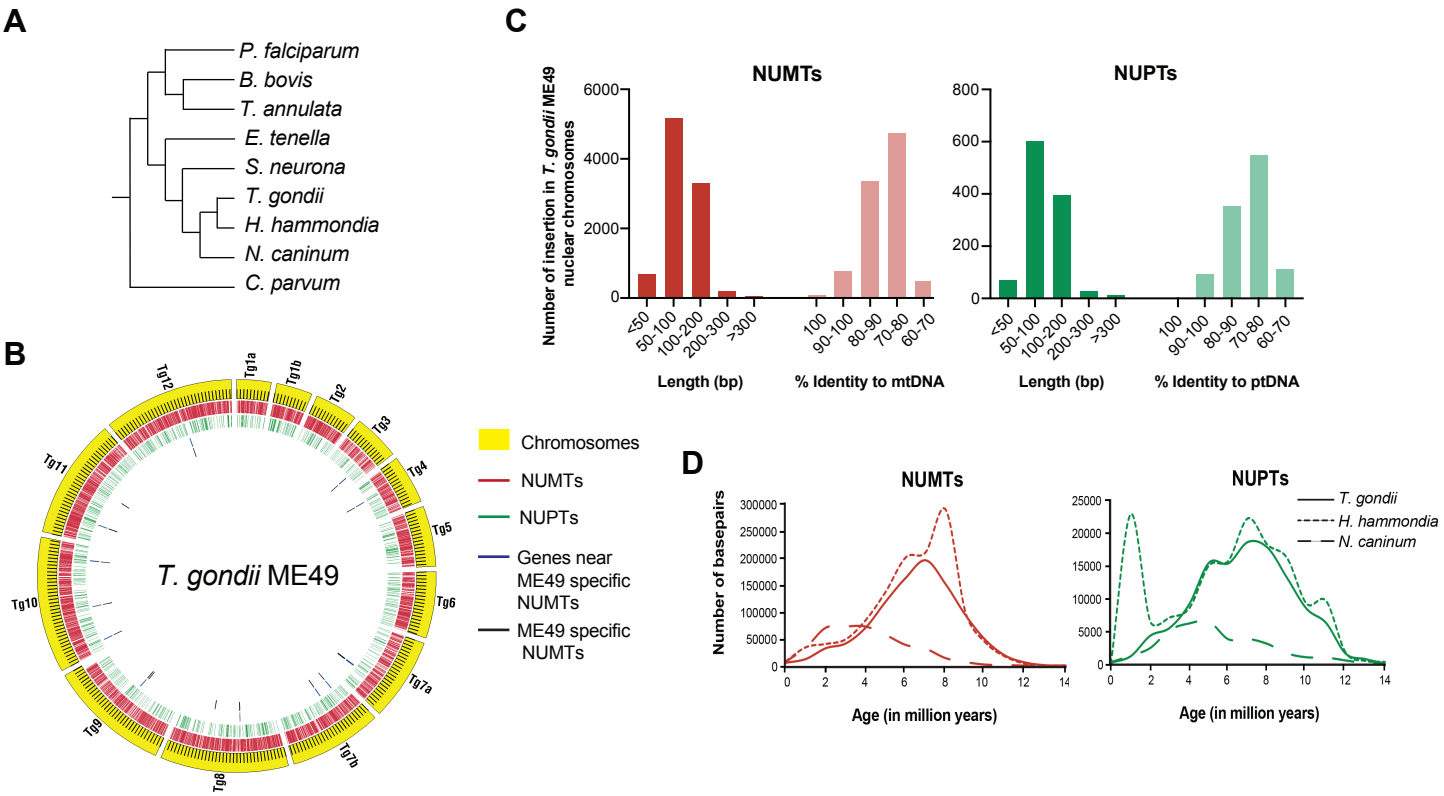
A
P. falciparum
B. bovis
T. annulata
E. tenella
S. neurona
T. gondii
H. hammondia
N. caninum
C. parvum
B
T. gondii ME49
Tg1a
Tg1b
Tg2
Tg3
Tg4
Tg5
Tg6
Tg7a
Tg7b
Tg8
Tg9
Tg10
Tg11
Tg12
Chromosomes
NUMTs
NUPTs
Genes near ME49 specific NUMTs
ME49 specific NUMTs
C
NUMTs
NUPTs
Number of insertion in T. gondii ME49 nuclear chromosomes
Length (bp)
% Identity to mtDNA
Length (bp)
% Identity to ptDNA
D
NUMTs
NUPTs
Number of basepairs
Age (in million years)
Age (in million years)
T. gondii
H. hammondia
N. caninum

Figure 2

A

```
TGGT1_chrVI   TGAAGCGAAGAAGAGAAATCGAAAAAAAAACGCAAGAGAGTGTAGACATTTAGCATCTGT  699307
TGME49_chrVI  TGAAGCGAAGAAGAGAAATCGAAAAAAAA-CGCGAGAGAGTG------------------
TGVEG_chrVI   TGAAGCGAAGAAGAGAAATCGAAAAAAAA-CGCGAGAGAGTG------------------

TGGT1_chrVI   CGTTAACATATGAGGATAAAAGGCAACTTTAAGCGCGGTATCAATACCTGCAGGATTGCT  699367
TGME49_chrVI  ------------------------------------------------------------
TGVEG_chrVI   ------------------------------------------------------------

TGGT1_chrVI   AGAACCATTTAAATGTAAATAGAGAGAGTGTGCACGCCCGCTGTTGCTGCGTCTTTCTTC  699427
TGME49_chrVI  ----------------------AGAGAGTGTGCACGCCCGCTGTTGCTGCGTCTTTCTTC
TGVEG_chrVI   ----------------------AGAGAGTGTGCACGCCCGCTGTTGCTGCGTCTTTCTTC
```

B

```
TGGT1_chrIV   TGTGCGACAGGTCCGTCAGCACATGCCTCGTCAAAAGAAAGGGGATTTCAGTATCCTA  1045199
TGME49_chrIV  TGTGCGACAGGTCCGTCAGCACATGCCTCGTCAAAAGAAAGGGGATTTCAGTATC---
TGVEG_chrIV   TGTGCGACAGGTCCGTCAGCACATGCCTCGTCAAAAGAAAGGGGATTTCAGTATCCTA

TGGT1_chrIV   CGGCACTCAGATTCTTCCACATCGGATTTGTTCTCGCGCAATACCTTGACTACTGTTA  1045259
TGME49_chrIV  ----------------------------------TCGCGCAGTACCTTGACTACTGTTA
TGVEG_chrIV   CGGCACTCAGATTCTTCCACATCGGATTTGTTCTCGCGCAATACCTTGACTACTGTTA
```

C

Clade	Chromosome	Ia	Ib		II	III	IV		V			VI			VIIa				VIIb					VIII			IX			X								XI										XII						
	NUMT #	1	2	3	4	5	6	7	8	9	10	11	12	13	14	15	16	17	18	19	20	21	22	23	24	25	26	27	28	29	30	31	32	33	34	35	36	37	38	39	40	41	42	43	44	45	46	47	48	49	50	51	52	53	54	55	56
A	CAST	+	-	+	-	+	-	-	-	-	+	+	+	-	+	+	+	+	-	+	-	-	+	+	+	-	-	+	+	+	-	+	+	+	+	-	+	-	-	+	+	-	-	-	-	+	-	+	-	+	+	-	+	-	-	+
	TgCtCo5	+	-	-	-	+	-	-	-	-	+	+	+	-	+	-	+	+	-	+	-	-	+	+	-	+	-	+	+	+	-	+	+	+	+	+	+	-	-	+	+	-	-	-	+	-	-	-	-	+	+	-	+	-	+	-
	GT1	+	-	+	+	+	-	-	-	-	+	+	+	-	+	+	-	+	-	+	-	-	+	+	-	+	-	+	+	+	-	+	+	+	+	-	+	-	+	+	+	+	-	-	+	-	-	-	+	-	+	-	+	-	-	+
	TgCATBr9	+	-	-	+	-	-	+	-	-	+	+	+	-	-	+	-	+	-	+	-	-	+	+	-	+	-	+	-	-	-	+	+	+	+	-	+	-	-	+	-	+	+	-	-	+	+	+	+	+	+	+	+	-	-	+
	GAB2	+	-	-	-	+	-	-	-	-	+	+	+	-	+	+	-	+	-	+	-	-	+	+	-	+	-	+	+	+	-	-	-	+	+	-	+	+	-	+	-	-	-	-	-	+	+	-	-	+	+	+	-	-	+	-
	FOU	+	-	-	+	+	-	-	-	-	+	+	+	-	+	+	-	+	-	+	-	-	+	+	-	+	-	+	+	+	-	+	+	+	+	-	+	-	-	+	-	+	-	-	-	+	+	-	+	+	+	+	+	-	+	-
B	TgCATBr5	+	-	-	+	+	-	+	-	-	-	+	+	-	-	+	+	+	+	+	-	-	+	+	-	-	-	+	-	-	-	+	+	-	+	-	+	-	+	+	+	+	+	+	+	-	+	-	+	-	+	+	+	-	-	+
	MAS	+	+	+	-	+	+	+	-	-	-	-	-	-	+	+	+	+	+	+	-	-	+	+	+	+	+	+	-	-	+	+	+	+	+	-	-	-	-	+	+	+	+	+	+	-	+	-	+	+	+	-	+	-	+	+
C	p89	+	+	-	-	+	-	-	-	-	+	+	+	+	+	-	+	+	-	+	-	-	+	+	+	-	-	+	+	+	-	+	+	-	+	-	-	-	+	-	+	+	-	+	-	+	-	+	-	+	+	+	-	+	+	-
	VEG	+	-	-	-	+	-	-	-	-	+	-	+	-	+	-	+	-	-	+	-	-	-	-	+	-	-	+	+	+	-	+	+	-	+	-	-	-	-	+	+	-	-	+	-	-	+	-	+	+	+	+	-	+	-	+
D	ME49	+	-	-	-	+	-	-	-	+	-	-	+	-	+	+	+	+	-	-	+	-	-	-	+	-	+	+	+	+	+	-	-	+	+	-	+	+	-	+	+	+	-	-	+	-	-	+	-	+	-	-	-	-	+	+	-	+
	ARI	+	+	-	-	+	-	-	-	+	-	-	+	-	+	+	+	+	-	-	+	-	-	-	+	-	+	+	+	+	+	-	+	-	+	-	+	-	-	+	+	-	-	-	+	-	-	-	-	+	+	-	-	+	+	-	+
	TgCat PRC2	+	+	-	-	+	-	-	+	-	-	-	+	-	+	+	+	+	-	+	+	+	+	+	+	-	+	+	+	+	+	+	+	+	+	-	+	-	-	+	+	-	-	-	+	-	+	-	-	+	+	-	-	-	+	+	+
	COUG	+	+	+	-	+	-	-	-	+	-	-	+	-	+	+	+	+	-	-	+	+	+	-	+	-	+	+	+	+	+	+	+	+	+	-	+	-	-	+	+	-	-	-	+	-	+	-	-	+	+	-	+	+	-	+
F	VAND	-	-	-	+	+	-	-	-	-	+	+	+	+	+	+	+	-	-	+	-	-	+	+	-	-	-	+	+	+	-	+	+	-	-	+	+	-	+	+	+	+	-	-	+	-	+	-	-	-	+	-	+	-	+	+	+
	RUB	-	+	-	+	+	-	-	-	-	+	+	+	-	+	+	-	+	-	+	-	-	+	+	+	+	-	+	+	+	-	+	+	+	+	-	+	-	-	+	+	+	-	-	+	-	+	-	-	-	+	-	+	-	-	-	+
% Divergence		14	20	8	2	2	0	1.9	6	16	0	1	23	0	26	28	15	31	0	15	27	2	23	21	22	23	14	29	29	21	24	18	22	18	14	0	23	0	25	19	26	2	0	5	24	0	24	12	25	3	3	23	1	25	0	20	0	14
Chromosome Location (TGME49)		1018474-1018944	213457-213857	1596582-1596989	261484-261902	2457884-2458465	1660519-1660918	2006407-2006806	1768829-1769234	2529301-2529857	2798255-2798857	706677-707077	2259261-2259751	2415880-2416280	605108-605597	2259268-2259788	2673706-2674160	3250336-3250897	668720-669119	1025866-1026297	1710159-1710710	1904265-1904665	3218491-3219027	4646913-4647351	2497086-2497686	3466455-3466854	4435378-4435833	3008823-3009336	3038491-3039017	4251589-4252066	4753118-475768	2699533-2699941	2977559-2977959	3011324-3011796	5158557-5159008	6191403-6191803	6399526-6400012	6727704-6728163	6863803-6864202	1532798-1533403	1603990-1604629	2153288-2153772	2168335-2168735	2292428-2293114	2922696-2929196	3138783-3139183	3380178-3380628	3550551-3551008	5020102-5020569	5133457-5133946	328834-329234	905189-905588	2430105-2430505	3864644-3865116	4009932-4010391	4599466-4599866	4641543-4642129

Figure 3

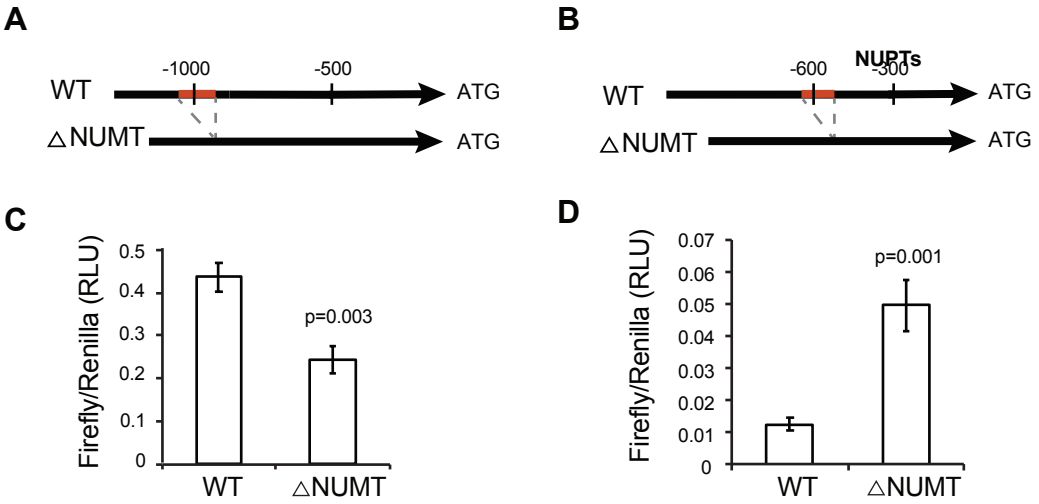
A
WT
-1000
-500
ATG
△NUMT
ATG
B
WT
-600
NUPTs
-300
ATG
△NUMT
ATG
C
Firefly/Renilla (RLU)
0.5
0.4
0.3
0.2
0.1
0
p=0.003
WT
△NUMT
D
Firefly/Renilla (RLU)
0.07
0.06
0.05
0.04
0.03
0.02
0.01
0
p=0.001
WT
△NUMT

Figure 4

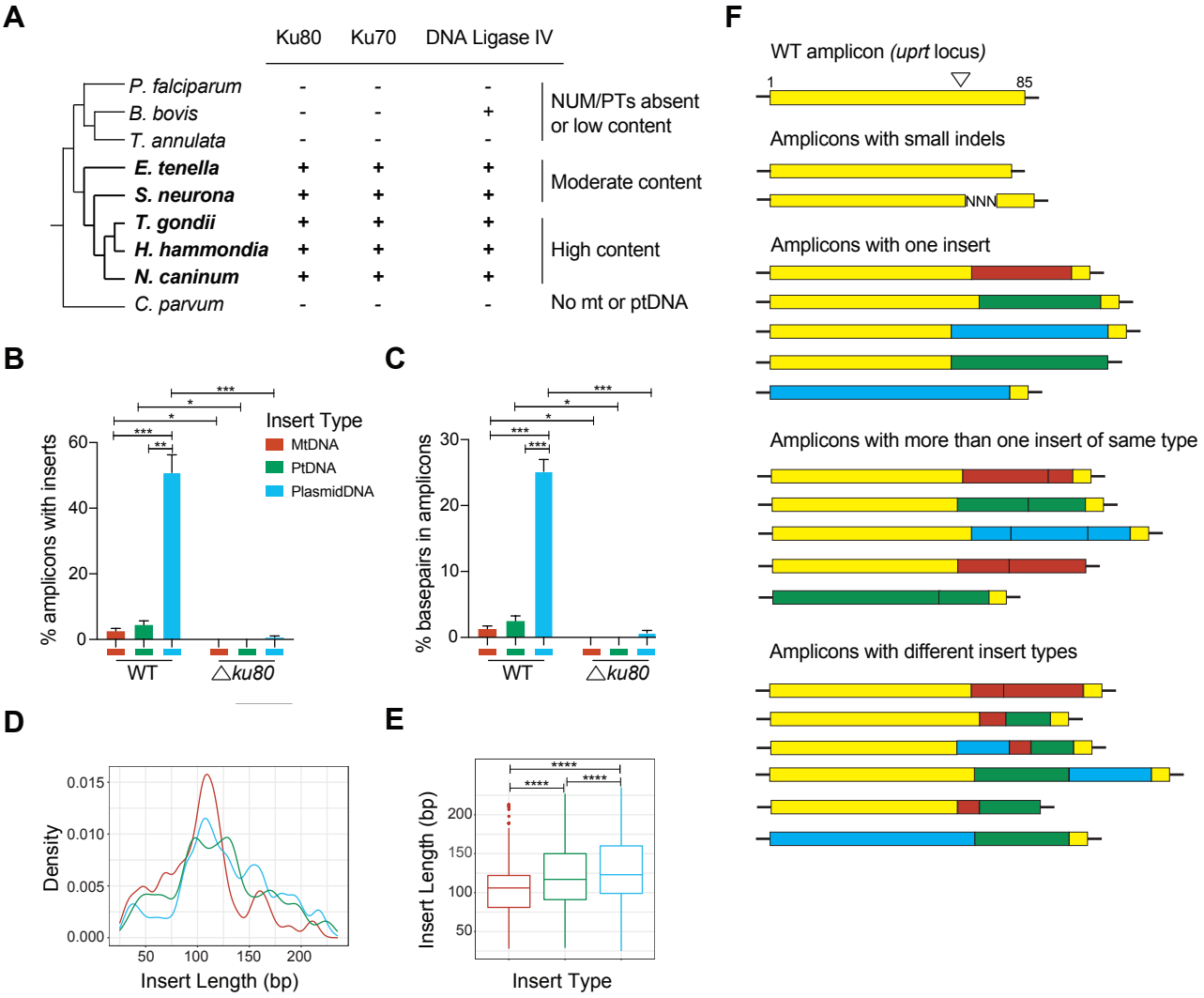
A
Ku80
Ku70
DNA Ligase IV
P. falciparum - - -
B. bovis - - +
T. annulata - - -
E. tenella + + +
S. neurona + + +
T. gondii + + +
H. hammondia + + +
N. caninum + + +
C. parvum - - -
NUM/PTs absent or low content
Moderate content
High content
No mt or ptDNA
B
% amplicons with inserts
Insert Type
MtDNA
PtDNA
PlasmidDNA
WT
△ku80
C
% basepairs in amplicons
D
Density
Insert Length (bp)
E
Insert Length (bp)
Insert Type
F
WT amplicon (uprt locus)
1
85
Amplicons with small indels
NNN
Amplicons with one insert
Amplicons with more than one insert of same type
Amplicons with different insert types

Supplementary Information for

Massive invasion of organellar DNA drives nuclear genome evolution in *Toxoplasma*

Sivaranjani Namasivayam[a 1] Cheng Sun[b 1] Assiatu B Bah[c] Jenna Oberstaller[d] Edwin Pierre Louis[e] Ronald Drew Etheridge[e] Cedric Feschotte[f] Ellen J. Pritham[c 2] and Jessica C. Kissinger[g 2]

To whom correspondence should be addressed. Email: jkissing@uga.edu

This PDF file includes:

Supplementary text
Figures S1 to S4
Tables S1 to S12
SI References

Other supplementary materials for this manuscript include the following:

Dataset S1 - Excel spreadsheet detailing each NUMT and NUPT insertion in *T. gondii* ME49

Supplementary Information Text

Supplementary Materials and Methods

DNA extraction and PCR

DNA from *T. gondii* RH and ME49 parasites was extracted using DNeasy Blood and Tissue Kit (Qiagen) following manufacturer's cultured cells protocol. PCR was performed using the following conditions using primers in Table S6: initial denaturation at 95˚C for 3 minutes; followed by 35 cycles of amplification at 95˚C for 60 seconds, 52.5˚C for 45 seconds, and 72˚C for 40 seconds. The PCR products were visualized using agarose gel electrophoresis.

Identification of NUMTs and NUPTs.

RepeatMasker version 4.0.5 (http://www.repeatmasker.org) rather than the frequently used BLASTN was used to identify organellar DNA sequences in the nuclear genomes as it provides better accuracy, handles many-to-one hits, avoids overestimates and provides a detailed annotation of the identified sequences, which facilitates subsequent characterization. Mitochondrial and apicoplast genome sequences were used as the "repeat library" and "cross_match" was used as the search engine, with filtering out low complexity sequences and other parameters as default, to mask the corresponding nuclear genomes to identify NUMTs and NUPTs respectively. For *T. gondii* and *N. caninum* the species-specific 21 sequence blocks as well as cytochrome coding sequences, *coxI*, *coxIII* and *cob* (1) were used to mask the corresponding assembled nuclear chromosomal sequences. Since the 21 sequence blocks occur in a number of random arrangements and a NUMT can arise from a non-contiguous mitochondrial sequence, the cytochrome sequences were included to minimize the overestimation of the number of NUMTs. The apicoplast sequence *T. gondii* (GenBank: U87145.2) was used to detect NUPTs in *T. gondii* ME49 and *N. caninum* Liverpool. Since the mtDNA sequence could not be distinguished from NUMTs in *H. hammondi* (ToxoDB.org) (2), *T. gondii* mtDNA sequences were used to identify NUMTs in *H. hammondi*. Additionally, the publicly available apicoplast sequence for *H. hammondi*

is incomplete in comparison to the well annotated plastid sequence of *T. gondii.* Therefore, *T. gondii's* apicoplast sequence was used to screen for NUPTs in *H. hammondi*. The partial cytochrome sequences annotated in *S. neurona* and *T. gondii* mtDNA sequences were used to identify NUMTs in *S. neurona* and the parasites' own apicoplast DNA sequence was used to identify NUPTs. NUMTs and NUPTs in *E. tenella* were detected using its own organellar genome sequences (GenBank Accessions: AB564272.1 and AY217738.1. Similarly, *Plasmodium, Babesia* and *Theileria* species-specific organellar sequences obtained from VEuPathDB.org were used to screen their respective nuclear chromosome sequences for NUOTs and genes involved in the NHEJ DSB repair pathway. NUOTs shorter than 28 bp and overlapping insertions were only counted once.

Identification of segmental duplications, shared and uniquely-present NUMTs

Segmental duplications were identified by extracting NUMT sequences along with 150 bp of the flanking regions. The extracted sequences were used as BLASTN queries against themselves. If a NUMT along with at least 100bp of flanking sequence was present at least twice it was counted as a segmental duplication (3).

Following the identification NUMTs in *T. gondii* ME49 reference nuclear genome, NUMTs were similarly identified in nuclear genomes of two other fully assembled *T. gondii* strains, GT1 and VEG using the same mtDNA library repeat described above. Subsequently, the *de novo* assembled genomes of 13 *T. gondii* strains namely, ARI, CAST, TgCtBr5, TgCtBr9, TgCtPRC2, COUG, TgCtCo5, FOU, GAB2-2007-GAL-DOM2, MAS, p89, RUB and VAND, were downloaded from ToxoDB.org (2) and NUMTs were similarly identified. It should be noted that the genomes of these 13 strains have not be assembled into chromosomes and occur as scaffolds and contigs. Therefore, NUMTs that are present at the ends of these sequences could not be included in the analyses due to the lack of flanking regions. Additionally, any scaffold or contig that contained only mitochondrial DNA sequence was not included in further analysis. In order to identify NUMTs that were shared or unique among the strains, each NUMT sequence along with 200 bp of flanking sequences from one strain was searched against the NUMTs with 200 bp flanking sequences of all other strains using BLASTN. For each pairwise comparison, the NUMT was considered to be shared only when >150 bp of the upstream and downstream flanking sequence was present. If both flanking sequences were not present, the match was not considered. NUMTs that were present in only one strain were called 'strain-specific *T. gondii* NUMTs' and NUMTs that present in more than one strain were called 'differentially present *T. gondii* NUMTs'. NUMTs that were present in all 16 strains were called 'shared *T. gondii* NUMTs'. Strain-specific NUMTs identified from the comparison of just the three fully-assembled strains ME49, GT1 and VEG were manually verified. Finally, a similar approach was utilized to identify NUMTs that were shared or uniquely present among *T. gondii* ME49 and *N. caninum*. All BLASTN search results were filtered for an E-value = 0 and query coverage of >90%.

Estimation of NUOT age

The relative date of insertion of a NUMT can be inferred from the NUMTs age. RepeatMasker reports a percent divergence between the NUMT and the corresponding mtDNA sequence. The percent divergences were converted into genetic distances using the Jukes-Cantor Model formula $K = -\frac{3}{4}\ln(1-\frac{4}{3}p)$, where K is the genetic distance and p is the percent divergence between the mtDNA and NUMT. Percent divergence was calculated by dividing the number of substitutions between the two sequences by the sequence length. Using the genetic distance the age of each NUMT was calculated using the formula, $T = K/2\mu$, where T is the age of the NUMT, K is the genetic distance (Dataset S1), μ is the intron mutation rate. The intron mutation rate was used to calculate the age of the NUMTs since NUMTs are not expected to be under selective pressure and should have a neutral mutation rate similar to the introns. The intron mutation rate was previously calculated as 2.12×10^{-8} (4). The same rate was for used for all three species.

Expression constructs and Transient Transfection.

PCR primers (Table S6) containing the attB1 and attB2 sites were used to amplify the appropriate promoter and 5′-UTR regions from ME49 genomic DNA for the two genes tested. A two-step

overlap-extension PCR technique (5) was employed to delete the NUMT sequence from each promoter. The Gateway™ cloning system (Invitrogen) was used to clone the WT and deletion promoters. These two kinds of promoters were first cloned into pDONR221 via the BP reaction. Following sequencing verification, these promoter fragments were moved into a firefly luciferase-expressing vector (destination vectors) via the LR reaction. As constitutive *T. gondii* promoter (α-tubulin)-driven renilla luciferase-expressing construct was co-transfected along with the experimental construct. Nucleotide positions in these deletion studies are referenced with respect to the start of translation (+1). Parasite culture and transient transfections were performed as described (6). In short, *T. gondii* RH tachyzoites were transiently transfected via electroporation. 18-24 hours post-electroporation the cells were scraped and lysed using passive lysis buffer (Promega, Madison, WI, USA) and a dual luciferase assay was performed on the extract using the Promega Dual Luciferase kit. The different substrate requirements for Firefly and Renilla luciferase allowed us to assay reporter expression for each construct sequentially within the same extract. Reporter activity from the WT or mutagenized promoter was measured relative to the internal control, eliminating errors due to variation in parasite populations and individual transfections. Each electroporation experiment was performed 6 times and luciferase assays were performed in duplicate for expression measurements. The unpaired Students *t*-test was used to calculate the statistically significant difference in expression levels between WT and mutagenized promoter activity; $p < 0.05$ was considered statistically significant.

CRISPR-Cas9 transfection assays, amplicon sequencing and analysis of inserts

T. gondii strains RH and an RH mutant TATiΔ*ku80*, referred here as WT and Δ*ku80* (7) respectively were cultured on human immortalized fibroblast (hTERT) cells grown in Dulbecco's Modified Eagle's Medium (DMEM) supplemented with 10% heat-inactivated Cosmic Calf Serum, 0.5% 10mg/ml penicillin-streptomycin and 0.05% 10 mg/ml gentamycin. *T. gondii* RH WT and Δ*ku80* parasites were filtered, washed and resuspended in cytomix (supplemented with ATP and glutamine) at a concentration of 3.3×10^7 parasites/ml. 10^7 parasites were electroporated with 8 µg of the CRISPR/Cas9 plasmid with a single guide RNA targeting the UPRT locus utilizing a BTX electroporator (CRISPR/Cas9 plasmid and guide RNA kindly provided by Michael Cipriano and Boris Striepen). hTERT cells were infected with the transfected parasites (WT or Δ*ku80* in triplicate) and grown for 48 hours without drug selection. After 48 hours, lysed parasites were passed to infect fresh hTERT cells and placed under 10 µM of 5-fluorodeoxyuridine (5-FUDR) drug selection to select for parasites with a mutation in the UPRT gene. Parasites were harvested following four rounds of drug selection and DNA was extracted using Qiagen Blood and Tissue kit following the manufacturer's protocol. PCR was performed using primers (Forward primer: 5′-TATGGTAATTGTGAAGTGACAACCCCTCTGGA-3′; Reverse primer: 5′-AGTCAGTCAGCCCAAGCCACTTTCCATCGACT-3′) targeting the UPRT locus to generate 66 bp amplicons from DNA extracted from all six transfections. Amplicons were then indexed and paired-end sequencing (PE 150 bp) was performed using the Illumina MiSeq sequencer.

Sequenced paired-end reads were filtered and trimmed using trimmomatic (minimum length:36, sliding window:4:20) (8), The processed paired-end reads were then merged using FLASH (default parameters) (8, 9). Following quality control and merging of paired-end reads unique reads were identified using the usearch fastx_uniques script (10). The unique reads were then investigated for the presence of *T. gondii* mtDNA (21 sequence blocks), ptDNA, and CRISPR/Cas9 plasmid DNA sequences using RepeatMasker and each genome sequence as a repeat library. RepeatMasker results were then analyzed to identify the characteristics of the inserts reported in Fig. 4.

Figures and Tables

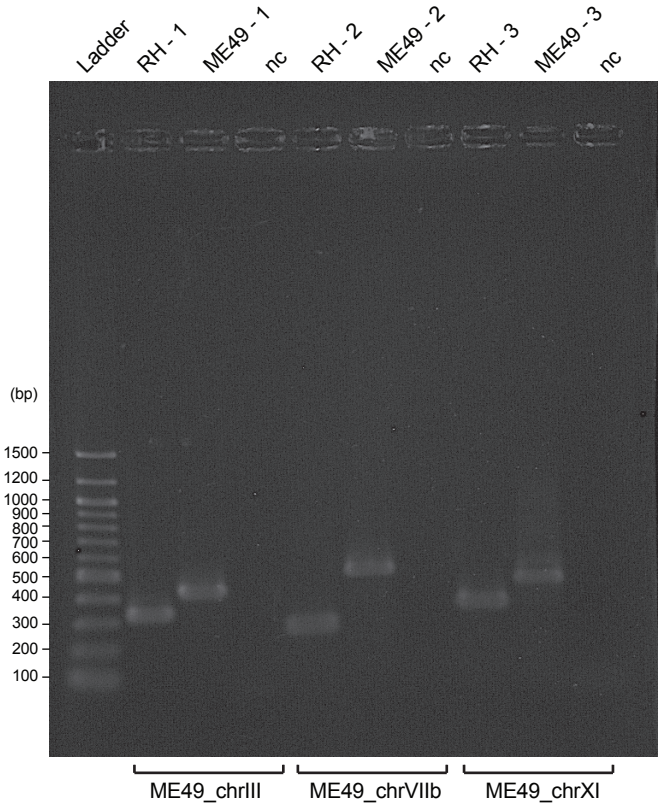

Figure S1. PCR verification of select strain-specific NUMTs. Genomic DNA from *T. gondii* strains ME49 and RH were assayed with three primers sets that each target a strain specific NUMT loci. The strain is indicated across the top and 'nc' denotes the negative control for each reaction. The primers are specified on the bottom and the primer sequences are provided Table S6. ME49_chrIII ME49_chrVIIb and ME49_chrXI correspond to NUMTs located at TGME49_chrIII:1730617..1730859, TGME49_chrV11b:1710367..1710510, and TGME49_chrXI:3550511..3550993 in Table S4 respectively. All NUMTs shown here are present in ME49 and absent in RH. RH was utilized instead of GT1 since RH is a widely used *T. gondii* strain in laboratory cultures. RH and GT1 are closely related strains. However ,a fully assembled genome sequence is unavailable.

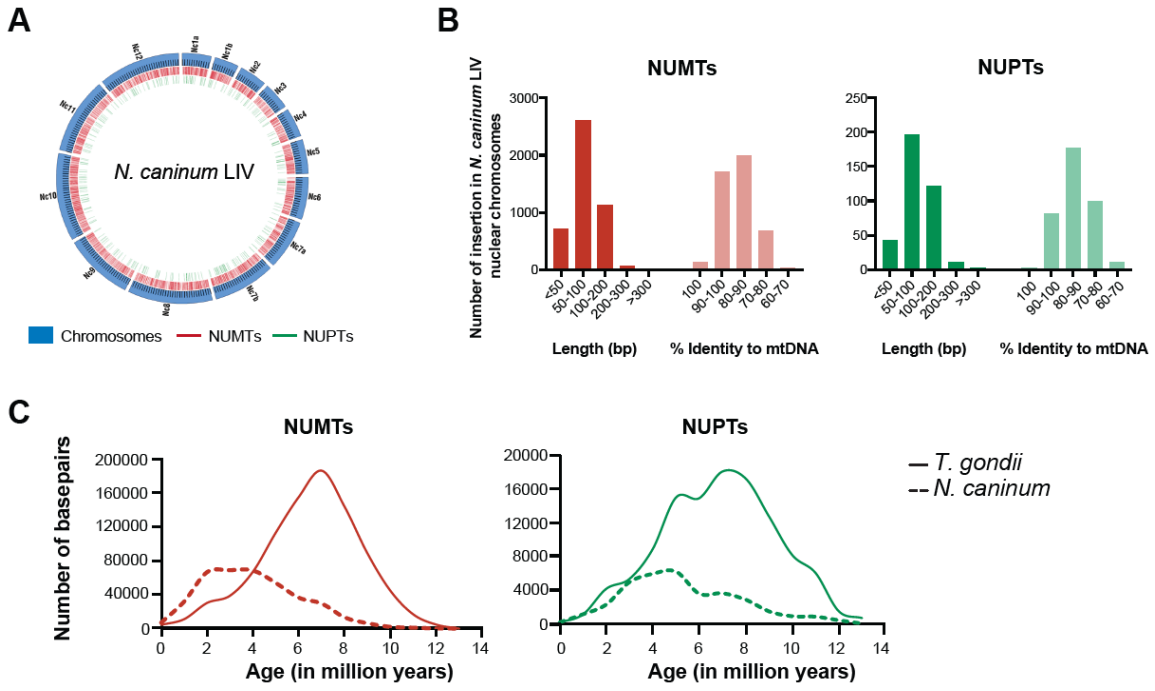

Figure S2. Characteristics of NUMTs and NUPTs in *N. caninum LIV* *(A)* Circos plot represents the distribution of NUMTs and NUPTs in the nuclear chromosomes of *N. caninum LIV*. The blue bands indicate the chromosomes as labeled and each tick on the band equals 100 kb. The ticks interior to the chromosomes are indicate the location of NUMTs and NUPTs as referenced in the key. *(B)* The length and the percent identity of a NUMT and NUPT to *N. caninum* mt and ptDNA respectively was calculated from RepeatMasker results and the distribution is plotted. *(C)* The age of each NUMT and NUPT was calculated based on the percent divergence from the mt and ptDNA as described in the Methods and the distribution of the age is plotted against the number of base pairs.

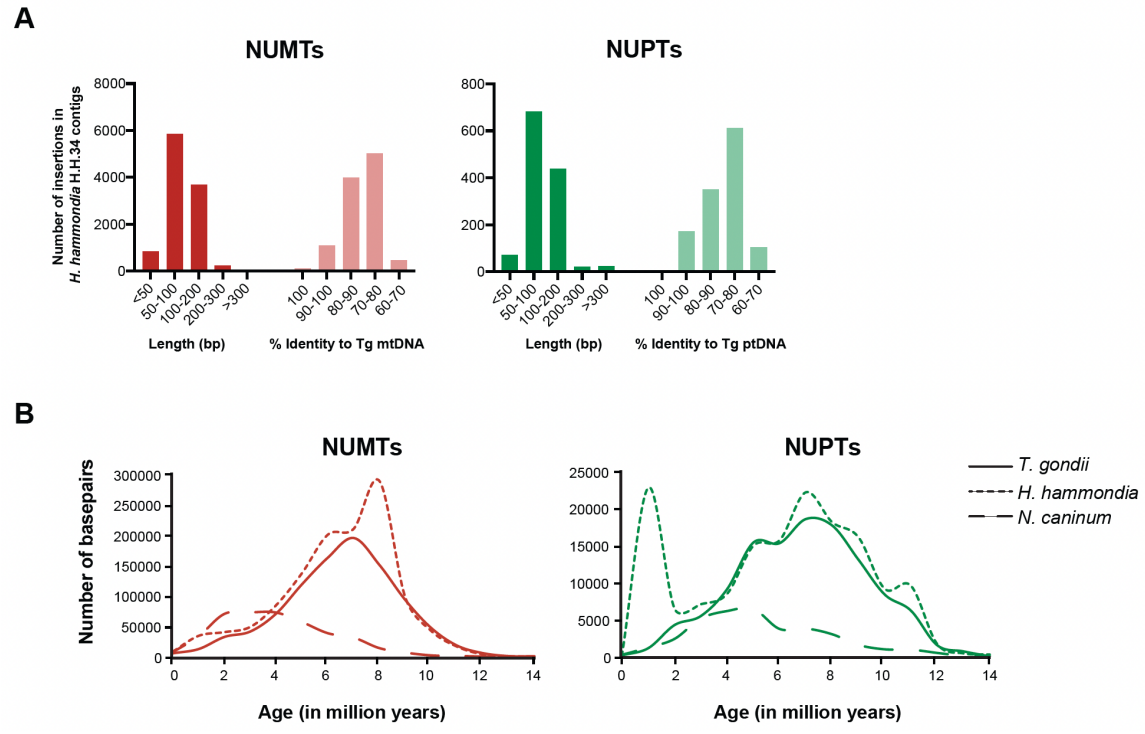

Figure S3. Characteristics of NUMTs and NUPTs in *H. hammondi* H.H.34. (A) The length and percent identity of a NUMT and NUPT to *T. gondii* mt and ptDNA respectively was calculated from RepeatMasker results and the distribution is plotted. (B) The age of each NUMT and NUPT was calculated based on the percent divergence from the mt and ptDNA as described in the Methods and the distribution of the age is plotted against the number of base pairs. It should be noted that the NUM/PT analysis in *H. hammondi* was performed on genome contigs as a chromosome assembly is unavailable. Thus, the spike in the number of NUPT base pairs at ~1 million years is likely due to the presence of unassembled apicoplast genome sequences.

A) Gene: TGME49_286560 U6 snRNA-associated Sm family protein

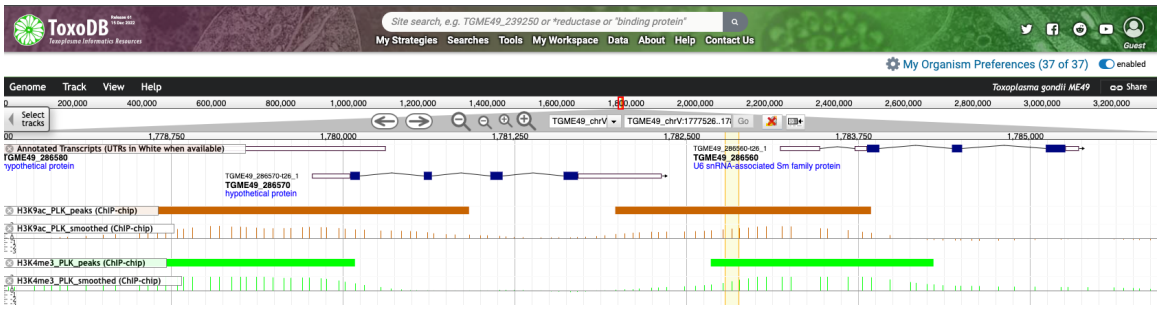

Sequence removed from the promoter region of TGME49_286560 U6 snRNA-associated Sm family protein gene was derived from mtDNA sequence block "U". The deleted sequence has a divergence of 28.8% from mtDNA sequence block U and an estimated divergence time 8.57 MYA. The sequence removed was: 5′ - GCAGCTAAATGCCACTAAAGCGAGGGAATTCTCGGTGTTCCCGTGTTCCCTGAAAGGTATTTGGAAGA

B) GENE: TGME49_254850 Myosin heavy chain

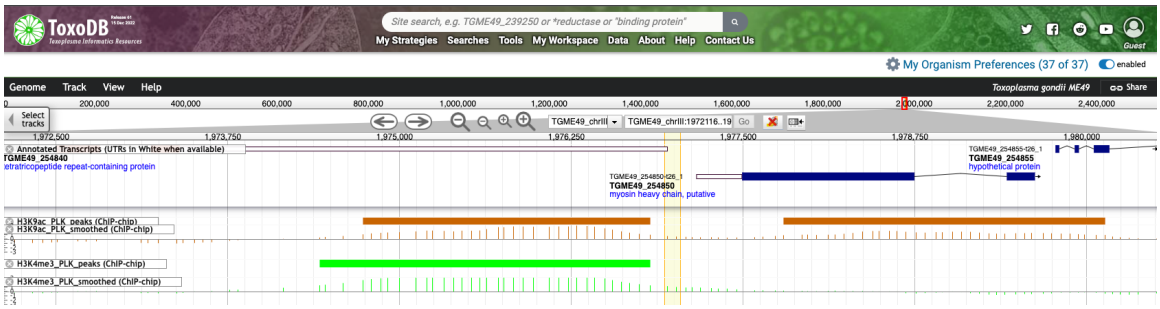

Sequence removed from the promoter region of TGME49_254850 putative myosin heavy chain gene was derived from bp 96-161 of mtDNA sequence block "F". The deleted sequence has 16.7% divergence from mtDNA sequence block F and an estimated divergence time 4.45 MYA. The sequence removed was: 5′ - CAACCCTGTATCATTTAACTCAGTTCTCTAGCAGTAGGTCTGGTATTCTGTACTAACCTATCTGAA

Figure S4. NUMT location and epigenetic marks for promoters used in transient *in vitro* reporter expression assays. (A) Promoter region of TGME49_286560 U6 snRNA-associated Sm family protein gene that shares an orthologous conserved NUMT derived from mtDNA sequence block "U" with *N. caninum*. (B) Promoter region of TGME49_254850 Myosin heavy chain gene that is not orthologous and was derived from mtDNA sequence block "F". Screen shots are from ToxoDB.org. Yellow highlight indicates the location of the NUMT. Orange and green data tracks represent H3K9ac and H3K4Me3 ChIP-chip data respectively. Both genes are located on the forward strand. The CDS is colored solid blue in the gene models. The uncolored regions on the ends of the gene models represent the 5′ and 3′ UTRs.

Table S1. Annotation of the 3,369 bp strain-specific NUMT on ChrX in *T.g.* ME49

Chromosome	Start	End	Divergence from mtDNA (%)	mtDNA gene/block	Start	End
TGME49_chrX	5732558	5732660	0	U	1	103
TGME49_chrX	5732662	5732907	1.6	coxIII	216	459
TGME49_chrX	5732891	5732976	0	O	1	86
TGME49_chrX	5732977	5733228	0	K	1	252
TGME49_chrX	5733227	5733447	0	cob	1	221
TGME49_chrX	5733451	5733767	0.3	coxIII	1	317
TGME49_chrX	5733697	5734062	0	coxI	11	376
TGME49_chrX	5734077	5734453	0.5	cob	20	396
TGME49_chrX	5734448	5734516	0	H	1	69
TGME49_chrX	5734467	5734581	0	coxI	1377	1491
TGME49_chrX	5734580	5734683	4.9	coxIII	216	317
TGME49_chrX	5734582	5734666	0	J	1	85
TGME49_chrX	5734667	5734752	0	O	1	86
TGME49_chrX	5734753	5734931	0	F	1	179
TGME49_chrX	5734932	5735016	0	R	1	85
TGME49_chrX	5735033	5735098	0	U	1	66
TGME49_chrX	5735100	5735284	0	coxIII	275	459
TGME49_chrX	5735285	5735354	0	M	457	526
TGME49_chrX	5735351	5735396	0	D	1	46
TGME49_chrX	5735397	5735508	0	K	334	445
TGME49_chrX	5735509	5735860	0	U	1	353
TGME49_chrX	5735862	5735926	0	coxIII	395	459

Table S2. Characteristics of the NUMTs generated from the 21 mtDNA blocks in *T. gondii* and *N. caninum*

Block	*T. gondii* ME49[a]								*N. caninum* LIV[a]								Entire block found at 100% identity in nuclear genome?	
	Length of block	# of NUMTs	# of bp	% of genome	Number of insertions based on % identity to mtDNA[b]				Length of block	# of NUMTs	# of bp	% of genome	Number of insertions based on identity to mtDNA[b]					
					100	>=90	>=80	>=70					100	>=90	>=80	>=70	*Tg*	*Nc*
A	196	298	24376	0.04	1	42	158	293	196	161	12205	0.02	6	65	136	161	N	N
B	40	31	1213	0.002	4	15	31	31	40	39	1538	0.002	6	31	39	39	Y	Y
C	1050	246	28107	0.04	2	26	84	223	1050	361	31440	0.05	6	110	291	357	N	N
D	82	181	11544	0.02	4	25	115	178	82	78	4710	0.008	3	48	75	78	N	N
E	683	829	88673	0.14	5	64	345	783	683	414	38823	0.07	16	168	333	410	N	N
F	179	308	25785	0.04	2	35	166	297	179	188	14559	0.03	4	74	163	188	Y	N
H	447	291	28704	0.05	1	36	123	274	447	162	13416	0.02	4	58	141	162	N	N
I	204	160	13483	0.02	1	21	92	152	204	71	5274	0.009	0	36	61	71	N	N
J	85	626	42485	0.07	5	68	385	624	85	303	18362	0.03	19	168	283	303	Y	Y
K	445	696	64432	0.1	6	69	334	668	445	292	24364	0.04	12	138	248	288	N	N
L	159	610	53125	0.08	3	45	288	588	159	278	21453	0.04	13	122	233	277	Y	Y
M	754	890	86617	0.14	9	87	393	836	754	406	37383	0.06	11	163	336	403	N	N
N	166	173	15536	0.02	0	14	78	170	166	123	9706	0.02	3	42	103	123	N	N
O	86	234	15987	0.03	3	33	137	234	86	130	8091	0.01	6	50	122	130	Y	Y
P	184	301	26339	0.04	0	43	159	281	184	146	11253	0.02	6	58	126	146	N	N
Q	65	62	3489	0.01	2	15	47	62	65	65	3498	0.006	2	38	62	65	Y	Y
R	85	161	10627	0.02	3	18	109	160	85	61	3820	0.006	1	32	56	61	Y	N
S	205	529	49330	0.08	4	56	234	495	205	293	22767	0.04	9	122	255	290	Y	Y
T	279	290	29359	0.05	1	25	126	272	278	157	13902	0.02	3	58	138	154	N	N
U	354	614	56972	0.09	9	70	293	585	354	306	25381	0.04	6	147	269	306	N	N
V	161	961	83655	0.13	7	87	489	943	161	461	35217	0.06	16	204	403	461	Y	N

[a] Analysis performed with only with 21 mtDNA blocks. Cytochromes gene sequences were not included in the repeat library.
[b] Insertion may not be of the entire element.

Table S3. Categorization of NUOTs by *T. gondii* ME49 genome feature

NUMT	Number of insertions	Number of bp	% of NUOT in each genomic feature	% of each feature in total genome
CDS	30	2,151	0.24	31.69
Intron	4,784	458,133	50.63	31.76
UTR	1,053	97,854	10.81	14.86
Within 1 kb upstream of gene	1,151	109,124	12.06	21.31
Within 1 kb downstream of gene	1,155	105,692	11.68	21.31
Further Intergenic	1,596	343,207	12.65	21.64
Overall*	9,379	895,312	1.43	100
NUPT				
CDS	4	430	0.38	31.69
Intron	724	74,995	66.70	31.76
UTR	95	8,824	7.85	14.86
Within 1 kb upstream of gene	80	7,168	6.37	21.31
Within 1 kb downstream of gene	103	9,875	8.78	21.31
Intergenic	86	10,448	9.29	21.64
Overall*	1,108	112,443	0.18	100.00

* NUMTs spanning more than one genomic feature are included only in 'Overall'

Table S4. NUM/PTs that show duplication in the nuclear genome sequence

NUMTs				NUPTs			
Chr	**Start**	**End**	**# of paralogs**	**Chr**	**Start**	**End**	**# of paralogs**
chrII	5099	5205	4	chrII	13814	13914	3
chrII	12415	12541	10	chrIX	4970045	4970847	2
chrII	2236834	2236938	10	chrIX	5043622	5044424	2
chrII	2248185	2248306	5	chrIa	15741	15841	3
chrII	2254771	2254900	10	chrIa	1573069	1573330	3
chrII	2282076	2282144	4	chrVIIb	3733927	3733976	2
chrII	2284315	2284383	4	chrVIIb	3768369	3768418	2
chrII	2297290	2297357	4	chrX	5380837	5380969	2
chrIII	2298160	2298288	5	chrX	5384909	5384985	2
chrIII	2311257	2311387	6	chrX	5385366	5385498	2
chrIII	2317828	2317934	9	chrXII	39449	39549	3
chrIII	2320846	2320956	5	chrXII	5075497	5075568	2
chrIII	2370825	2370882	2	chrXII	5082862	5082947	2
chrIII	2370882	2370943	2				
chrIII	2393190	2393267	2				
chrIII	2465531	2465659	6				
chrIII	2474207	2474318	5				
chrIV	2255933	2256057	4				
chrIX	60905	61059	2				
chrIX	63920	64026	2				
chrIX	68225	68293	2				
chrIX	123864	123919	2				
chrIX	125504	125559	2				
chrIX	139089	139138	2				
chrIX	139140	139238	2				
chrIX	139933	139982	2				
chrIX	139984	140082	2				
chrIX	1205849	1205934	2				
chrIX	1205938	1206058	2				
chrIX	1206053	1206114	2				
chrIX	1215388	1215485	2				
chrIX	1215489	1215609	2				
chrIX	1215604	1215662	2				
chrIX	5043630	5043703	3				
chrIX	6271844	6271919	2				
chrIX	6271919	6271982	2				
chrIX	6295817	6295894	2				

chrIX	6312190	6312336	2
chrIX	6323557	6323643	4
chrIa	7040	7146	4
chrIa	14339	14468	10
chrIa	1573249	1573322	3
chrIb	1938127	1938216	3
chrIb	1942780	1942869	3
chrIb	1949100	1949189	3
chrV	4968	5026	3
chrV	5039	5130	2
chrV	13285	13376	2
chrV	92024	92125	4
chrV	113590	113715	3
chrV	509754	509812	4
chrV	509920	509997	4
chrV	1505158	1505214	2
chrV	1505226	1505333	2
chrV	1505382	1505487	3
chrV	3188040	3188109	2
chrV	3200304	3200423	2
chrV	3239267	3239336	2
chrV	3270617	3270756	2
chrVI	1701827	1701893	2
chrVI	3649599	3649705	4
chrVIIa	1527747	1527808	2
chrVIIa	1528989	1529050	2
chrVIIb	64268	64353	2
chrVIIb	67562	67630	2
chrVIIb	3750077	3750190	2
chrVIIb	3750271	3750393	2
chrVIIb	3750867	3751284	2
chrVIIb	3778763	3778876	2
chrVIIb	3778960	3779082	2
chrVIIb	3779556	3779973	2
chrX	5029	5140	6
chrX	8053	8120	10
chrX	56325	56431	8
chrX	63034	63093	5
chrX	140461	140567	4
chrX	140630	140698	8
chrX	143057	143119	2
chrX	4765609	4765669	2
chrX	4776491	4776552	2

chrX	4996027	4996088	2
chrX	5004771	5004832	2
chrX	7326929	7326985	3
chrX	7331267	7331323	3
chrX	7335390	7335442	3
chrXI	6008	6118	6
chrXI	8972	9078	10
chrXI	49359	49417	2
chrXI	51449	51507	2
chrXI	5597962	5598065	3
chrXI	5619174	5619266	2
chrXI	5619340	5619443	3
chrXII	30743	30849	4
chrXII	38049	38175	10
chrXII	565829	565894	2
chrXII	570379	570430	2
chrXII	1401437	1401499	2
chrXII	5688402	5688464	3
chrXII	5688465	5688515	3
chrXII	5693067	5693129	3
chrXII	5693130	5693180	3
chrXII	5695122	5695184	3
chrXII	5695185	5695235	3
chrXII	7055332	7055442	6
chrXII	7078152	7078309	3

Table S5. Strain-specific NUMTs in ME49 GT1 and VEG

Coordinates of NUMTs[a]	Divergence (%)	Associated nuclear gene	Location in gene	Only present /absent in	Insertion/ deletion
TGGT1_chrII: 244462..244554	4.4	TGGT1_221330	intron	GT1	insertion
TGGT1_chrII: 1102510..1102622	27.4	TGGT1_222410	1.8 Kb upstream	ME49	deletion
TGME49_chrIII: 1730617..1730859	23.5	TGME49_254420	intron	ME49	not sure
TGME49_chrIV: 1102974..1103065	20.6	TGME49_318770	1.3 Kb upstream	VEG	deletion
TGME49_chrIX: 2923871..2923932	3.2	none	none	ME49	insertion
TGME49_chrIX: 3047280..3047543	12.5	TGME49_289180	intron	VEG	deletion
TGGT1_chrVI: 699247..699347	1	TGGT1_239480	intron	GT1	insertion
TGGT1_chrVIII: 3463130..3463400	24.5	TGGT1_273478	intron	GT1	not sure
TGME49_chrVIII: 4435556..4435633	20.8	none	none	ME49	not sure
TGGT1_chrVIIa: 2687959..2688077	7.6	TGGT1_203135	intron	VEG	not sure
TGME49_chrVIIa: 3250536..3250697	30.6	TGME49_202540	1.3 Kb upstream	VEG	deletion
TGGT1_chrVIIb: 1000247..1000321	14.7	TGGT1_262780	173 bp downstream	ME49	deletion
TGGT1_chrVIIb: 3183923..3184103	23.2	none	none	GT1	not sure
TGGT1_chrVIIb: 4560651..4560737	21.2	TGGT1_255890	intron	GT1	not sure
TGME49_chrX: 475518..475568	23.5	TGME49_228230	3′ UTR	ME49	not sure
TGGT1_chrX: 2610785..2610846	17.7	TGGT1_224900	591 bp upstream	ME49	deletion
TGGT1_chrX: 2885685..2885842	24.1	TGGT1_224540B	intron	ME49	deletion
TGME49_chrX: 3011523..3011876	16.9	TGME49_224510	257 bp downstream	VEG	deletion
TGME49_chrX: 6399715..6399810	21.3	TGME49_014600	intron	VEG	deletion
TGGT1_chrX: 6755042..6755100	25.4	TGGT1_215260	intron	GT1	not sure
TGGT1_chrXI: 4963753..4963855	25.2	none	none	GT1	not sure
TGGT1_chrXII: 287472..287613	22.7	TGGT1_299820	1.1 Kb upstream	ME49	not sure
TGGT1_chrXII: 2346630..2346730	21.7	none	none	GT1	not sure
TGGT1_chrXII: 2367574..2367660	25.3	TGGT1_245610	intron	GT1	not sure

TGME49_chrVIII: 2496663..2496886	19.1	TGME49_233200	1.1 Kb upstream	GT1	deletion
TGME49_chrVIIa: 3199077..3199253	22.5	TGME49_202580	intron	VEG	deletion
TGME49_chrVIIb: 701168..701236	24.6	TGME49_263220	intron	ME49	not sure
TGME49_chrVIIb: 1710367..1710510	25	TGME49_261490	intron	ME49	not sure
TGME49_chrXI: 1310258..1310322	24.6	TGME49_310380	intron	GT1	deletion
TGME49_chrXI: 3550511..3550993	19.4	TGME49_313620	400 bp upstream	GT1	deletion
TGME49_chrXII: 3864844..3864916	0	TGME49_248450	intron	GT1	not sure

[a]Includes NUMTs that are partially present or absent in the other strain

Table S6. Primers used in Figure S1 and to amplify and alter the promoters used in the transfection assays (Fig. 3)

Primer	Sequence
ME49_chrIII (forward)	5'-GACTAGAGAAAGCCAAGGTAGCAC-3'
ME49_chrIII (reverse)	5'-GAATTCCCTGTTGCACACTATAAA C-3'
ME49_chrVIIb (forward)	5'-CGTCGAGTACATGAAAGTAAAGGTT-3'
ME49_chrVIIb (reverse)	5'-CAGGAAGACCACAAGAGAGAGAAG-3'
ME49_chrXI (forward)	5'-TATGTTTTTGTTTCGATGCTCAAG-3'
ME49_chrXI (reverse)	5'-GCGTTTTAGTACGCTCATTGTAAT C-3'
Sm family protein gene WT promoter (forward)	5'-GGGGACAAGTTTGTACAAAAAAGCAGGCTAATGTTGCCTACGGTTCTGACTA-3'
Sm family protein gene WT promoter (reverse)	5'-GGGGACCACTTTGTACAAGAAAGCTGGGTCCATTATGTCTAACTCCAGGAGGT-3'
Delete numt Sm family protein gene (forward)	5'-GGCAGTTGCATTCCAACATTTGATACTGCTAATGCTCTGCGGTAATAGA-3'
Delete numt Sm family protein gene (reverse)	5'-ATTATGTACCTCCTCTATTACCGCAGAGCATTAGCAGTATCAAATG-3'
Myosin heavy chain gene WT promoter (forward)	5'-GGGGACAAGTTTGTACAAAAAAGCAGGCTAACACCAGTGCGGGAGGCGTTCTAG-3'
Myosin heavy chain gene WT promoter (reverse)	5'-GGGGACCACTTTGTACAAGAAAGCTGGGTCCATTGTTTTCGAGCAGAGACATT-3'
Delete numt in myosin heavy chain gene (forward)	5'-TCCAGTTGAACTGCTCCTCTTTCTCTGTGTTCAATTATATTTGGGTGTA-3'
Delete numt in myosin heavy chain gene (reverse)	5'-ACTAGGAATCCTCCGATACACCCAAATATAATTGAACACAGAGAA-3'

Table S7. NUMT content in *T. gondii* strains

Species	Density (%)	Number of insertions	Number of base pairs
T. gondii GT1	1.44	9 175	874 525
T. gondii VEG	1.41	9 270	883 437
T. gondii CAST	1.39	9 370	876 895
T. gondii TgCtCo5	1.4	9 411	874 358
T. gondii TgCATBr9	1.42	9 332	874 826
T. gondii GAB2	1.4	9 373	880 313
T. gondii FOU	1.41	9 314	871 351
T. gondii TgCATBr5	1.41	9 370	869 048
T. gondii MAS	1.42	9 318	874 616
T. gondii p89	1.41	9 314	875 326
T. gondii ME49	1.43	9 379	895 312
T. gondii ARI	1.4	9 445	883 577
T. gondii TgCat_PRC2	1.4	9 485	880 946
T. gondii COUG	1.39	9 525	884 389
T. gondii VAND	1.41	9 331	879 564
T. gondii RUB	1.41	9 426	880 485

Table S8. Location of NUMTs displaying differential presence/absence in 16 *T. gondii* strains

Numt #[$]	Length (bp)	% Div	ME49 chr	Start*	End*	CAST	TgCTCo5	GT1	TgCATBr9	GAB2	FOU	TgCATBr5	MAS	p89	VEG	ME49	ARI	TgCat_PRC2	COUG	VAND	RUB	Location*	Associated gene
1	61	14	chrIa	1018474	1018944	1	1	1	1	1	1	1	1	1	1	1	1	1	1	0	0	I	294630
2	73	20	chrIb	213457	213857	0	0	0	0	0	0	0	1	1	0	0	1	1	1	0	1	UF	207690
3	67	7.7	chrIb	1596582	1596989	1	0	1	0	0	0	0	1	0	0	0	0	0	1	0	0	I	209970
4	45	2.3	chrII	261484	261902	0	0	1	1	0	1	1	0	0	0	0	0	0	0	1	1	I	221330
5	67	1.5	chrIII	2457884	2458465	1	1	1	0	1	1	1	1	1	1	1	1	1	1	1	1	IG	
6	28	0	chrIV	1660519	1660918	0	0	0	0	0	0	0	1	0	0	0	0	0	0	0	0	E	211630
7	157	1.9	chrIV	2006407	2006806	0	0	0	1	0	0	1	1	0	0	0	0	0	0	0	0	DF	210960
8	63	6.2	chrV	1768829	1769234	0	0	0	0	0	0	0	0	0	0	0	0	1	0	0	0	E	286590
9	51	16	chrV	2529301	2529857	0	0	0	0	0	0	0	0	0	0	1	1	0	1	0	0	I	285210
10	52	0	chrV	2798255	2798857	1	1	1	1	1	1	0	0	1	1	0	0	0	0	1	1	I	284170
11	100	1	chrVI	706677	707077	1	1	1	1	1	1	1	0	1	0	0	0	0	0	1	1	I	239480
12	91	23.3	chrVI	2259261	2259751	1	1	1	1	1	1	1	0	1	1	1	1	1	1	1	1	E	242770
13	64	0	chrVI	2415880	2416280	0	0	0	0	0	0	0	0	1	0	0	0	0	0	1	0	UF	243140
14	88	26.1	chrVIIa	605108	605597	1	1	1	0	1	1	0	1	1	1	1	1	1	1	1	1	I	304650
15	133	27.8	chrVIIa	2259268	2259788	1	0	1	1	1	1	1	1	0	0	1	1	1	1	1	1	I	203760
16	54	14.6	chrVIIa	2673706	2674160	1	1	0	1	0	0	1	1	1	1	1	1	1	1	1	0	DF	203220
17	162	30.6	chrVIIa	3250336	3250897	1	1	1	1	1	1	1	1	1	0	1	1	1	1	0	1	E	202540
18	59	0	chrVIIb	668720	669119	0	0	0	0	0	0	1	1	0	0	0	0	0	0	0	0	I	263270
19	75	14.7	chrVIIb	1025866	1026297	1	1	1	1	1	1	1	1	1	1	0	0	1	0	1	1	I	262780
20	140	26.5	chrVIIb	1710159	1710710	0	0	0	0	0	0	0	0	0	0	1	1	1	1	0	0	I	261490

21	53	1.9	chrVIIb	1904265	1904665	0	0	0	0	0	0	0	0	0	0	0	0	1	1	0	0	IG	
22	181	23.2	chrVIIb	3218491	3219027	1	1	1	1	1	1	1	1	1	0	0	0	1	1	1	1	IG	
23	87	21.2	chrVIIb	4646913	4647351	1	1	1	1	1	1	1	1	1	0	0	0	1	0	1	1	I	255890
24	77	22.1	chrVIII	2496611	2497086	1	0	0	0	0	0	0	1	1	1	1	1	1	1	0	1	IG	
25	99	23.2	chrVIII	3466455	3466854	0	1	1	1	1	1	0	1	0	0	0	0	0	0	0	1	I	243482
26	56	14.3	chrVIII	4435378	4435833	0	0	0	0	0	0	0	1	0	0	1	1	1	1	0	0	DF	271740
27	100	28.6	chrIX	3008823	3009336	1	1	1	1	1	1	1	1	1	1	1	1	1	0	1	1	I	289120
28	133	29.3	chrIX	3038491	3039017	1	1	1	0	1	1	0	0	1	1	1	1	1	1	1	1	I	289170
29	73	20.6	chrIX	4251589	4252066	1	1	1	0	1	1	0	0	1	1	1	1	1	1	1	1	IG	
30	51	23.5	chrX	475318	475768	0	0	0	0	0	0	0	1	0	0	1	1	1	1	0	0	E	228230
31	162	17.7	chrX	2699533	2699941	1	1	1	1	0	1	1	1	1	1	0	0	1	1	1	1	UF	224900
32	81	21.9	chrX	2977559	2977959	1	1	1	1	0	1	1	1	1	1	0	1	1	1	1	1	I	224540
33	74	17.6	chrX	3011324	3011796	1	1	1	1	1	1	0	1	0	0	1	0	1	1	0	1	I	224510
34	52	13.5	chrX	5158557	5159008	1	1	1	1	1	1	1	1	1	1	1	1	1	1	0	1	I	235920
35	78	0	chrX	6191403	6191803	0	1	0	0	0	0	0	0	0	1	0	0	0	0	1	0	I	214260
36	84	23.2	chrX	6399526	6400012	1	1	1	1	1	1	1	0	0	0	1	1	1	1	1	1	I	214600
37	59	0	chrX	6727704	6728163	0	0	0	0	1	0	0	0	0	0	1	0	0	0	0	0	UF	215060
38	58	25.4	chrX	6863803	6864202	0	0	1	0	0	0	1	0	1	0	0	0	0	0	1	0	I	215260
39	166	19.4	chrXI	1532798	1533403	1	1	1	1	1	1	1	1	0	1	1	1	1	1	1	1	DF	310710
40	239	25.8	chrXI	1603990	1604629	1	1	1	0	0	0	1	1	1	1	1	1	1	1	1	1	DF	310802
41	85	2.4	chrXI	2153288	2153772	0	0	1	1	0	1	1	1	1	0	1	0	0	0	1	1	IG	
42	48	0	chrXI	2168335	2168735	0	0	0	0	0	0	1	1	0	0	0	0	0	0	0	0	I	311625
43	57	5.2	chrXI	2292428	2293114	0	0	0	0	0	0	1	1	0	0	0	0	0	0	0	0	E	311800
44	102	24	chrXI	2928696	2929196	0	1	1	0	0	0	1	1	1	1	1	1	1	1	1	1	I	312820
45	37	0	chrXI	3138783	3139183	0	0	0	1	1	1	0	0	0	0	0	0	0	0	0	0	E	313150
46	122	24.1	chrXI	3380178	3380628	1	0	0	1	1	1	1	1	1	0	0	0	1	1	1	1	I	313430
47	58	12.1	chrXI	3550551	3551008	0	0	0	0	0	0	0	0	0	1	1	0	0	0	0	0	I	313630

48	103	25.2	chrXI	5020102	5020569	1	0	1	1	0	1	1	1	1	0	0	0	0	0	0	0	I	315845
49	38	2.6	chrXI	5133457	5133946	0	1	0	1	1	1	0	1	0	1	1	1	1	1	0	0	E	316100
50	142	22.7	chrXII	328834	329234	1	1	1	1	1	1	1	1	1	1	0	1	1	1	1	1	UF	299820
51	84	1.2	chrXII	905189	905588	0	0	0	1	1	1	1	0	1	1	0	0	0	0	0	0	I	219500
52	79	25	chrXII	2430105	2430505	1	1	1	1	0	1	1	1	1	0	0	0	0	1	1	1	I	245610
53	73	0	chrXII	3864644	3865116	0	0	0	0	0	0	0	0	0	1	1	1	0	1	0	0	I	248450
54	60	20	chrXII	4009932	4010391	0	0	0	0	1	1	0	0	1	1	1	1	1	1	1	0	UF	248580
55	35	0	chrXII	4599466	4599866	0	1	0	0	1	1	0	1	1	0	0	0	1	0	1	0	I	249530
56	41	13.7	chrXII	4641543	4642129	1	0	1	1	0	0	1	1	0	1	1	1	1	1	1	1	I	249560

[$]Only NUMTs that are present/absent almost entirely are included.

* Location of NUMT is with respect to the ME49 genome sequence. Start and stop co-ordinates include 200 bp up and downstream of NUMT. Genomic locations are indicated as Exon = E Intron = I Upstream flank = UF downstream flank = DF Intergenic = IG (intergenic does not include flanking regions). Coordinates for NUMT location include 200 bp upstream and downstream flanking regions of the NUMT. Presence =1 absence 0.

Table S9. Enrichment analyses of genes associated with NUMTs displaying differential presence/absence

ID	Name	Bgd count	Result count	Result gene list	Pct of bgd	Fold enrich-ment	Odds ratio	P-value	Benjamini	Bon-ferroni
GO:0007017	microtubule-based process	72	4	TGME49_209970 TGME49_235920 TGME49_243482 TGME49_315845	5.6	7.95	9.34	0.001465	0.18598	0.221162
GO:0007018	microtubule-based movement	46	3	TGME49_235920 TGME49_243482 TGME49_315845	6.5	9.33	10.77	0.003861	0.18598	0.583045
GO:0006928	movement of cell or subcellular component	49	3	TGME49_235920 TGME49_243482 TGME49_315845	6.1	8.76	10.06	0.00462	0.18598	0.69761
GO:0006071	glycerol metabolic process	2	1	TGME49_263270	50	71.51	146.3	0.013936	0.18598	1
GO:0046116	queuosine metabolic process	2	1	TGME49_316100	50	71.51	146.3	0.013936	0.18598	1
GO:0019400	alditol metabolic process	2	1	TGME49_263270	50	71.51	146.3	0.013936	0.18598	1
GO:0008616	queuosine biosynthetic process	2	1	TGME49_316100	50	71.51	146.3	0.013936	0.18598	1
GO:0023052	signaling	84	3	TGME49_202540 TGME49_215060 TGME49_289170	3.6	5.11	5.67	0.020239	0.18598	1
GO:0007165	signal transduction	84	3	TGME49_202540 TGME49_215060 TGME49_289170	3.6	5.11	5.67	0.020239	0.18598	1
GO:0055086	nucleobase-containing small molecule metabolic process	85	3	TGME49_215260 TGME49_289170 TGME49_316100	3.5	5.05	5.6	0.02088	0.18598	1

GO:0018130	heterocycle biosynthetic process	153	4	TGME49_215260 TGME49_249560 TGME49_289170 TGME49_316100	2.6	3.74	4.19	0.020974	0.18598	1
GO:0007154	cell communication	86	3	TGME49_202540 TGME49_215060 TGME49_289170	3.5	4.99	5.53	0.021533	0.18598	1
GO:1901362	organic cyclic compound biosynthetic process	158	4	TGME49_215260 TGME49_249560 TGME49_289170 TGME49_316100	2.5	3.62	4.05	0.023304	0.18598	1
GO:0006207	'de novo' pyrimidine nucleobase biosynthetic process	4	1	TGME49_215260	25	35.76	48.75	0.027683	0.18598	1
GO:0051716	cellular response to stimulus	170	4	TGME49_202540 TGME49_210960 TGME49_215060 TGME49_289170	2.4	3.37	3.75	0.029529	0.18598	1
GO:0046785	microtubule polymerization	5	1	TGME49_209970	20	28.61	36.55	0.034486	0.18598	1
GO:0046112	nucleobase biosynthetic process	5	1	TGME49_215260	20	28.61	36.55	0.034486	0.18598	1
GO:0042455	ribonucleoside biosynthetic process	5	1	TGME49_316100	20	28.61	36.55	0.034486	0.18598	1
GO:0009112	nucleobase metabolic process	5	1	TGME49_215260	20	28.61	36.55	0.034486	0.18598	1
GO:0034404	nucleobase-containing small molecule biosynthetic process	5	1	TGME49_316100	20	28.61	36.55	0.034486	0.18598	1
GO:1901659	glycosyl compound biosynthetic process	5	1	TGME49_316100	20	28.61	36.55	0.034486	0.18598	1

GO:0007020	microtubule nucleation	5	1	TGME49_209970	20	28.61	36.55	0.034486	0.18598	1
GO:0019856	pyrimidine nucleobase biosynthetic process	5	1	TGME49_215260	20	28.61	36.55	0.034486	0.18598	1
GO:0009190	cyclic nucleotide biosynthetic process	5	1	TGME49_289170	20	28.61	36.55	0.034486	0.18598	1
GO:0009187	cyclic nucleotide metabolic process	5	1	TGME49_289170	20	28.61	36.55	0.034486	0.18598	1
GO:0009163	nucleoside biosynthetic process	5	1	TGME49_316100	20	28.61	36.55	0.034486	0.18598	1
GO:0006206	pyrimidine nucleobase metabolic process	5	1	TGME49_215260	20	28.61	36.55	0.034486	0.18598	1
GO:0031109	microtubule polymerization or depolymerization	5	1	TGME49_209970	20	28.61	36.55	0.034486	0.18598	1
GO:0009119	ribonucleoside metabolic process	6	1	TGME49_316100	16.7	23.84	29.24	0.041244	0.207656	1
GO:0050896	response to stimulus	189	4	TGME49_202540 TGME49_210960 TGME49_215060 TGME49_289170	2.1	3.03	3.35	0.041256	0.207656	1
GO:0034654	nucleobase-containing compound biosynthetic process	117	3	TGME49_249560 TGME49_289170 TGME49_316100	2.6	3.67	4	0.047299	0.226289	1
GO:0097435	supramolecular fiber organization	7	1	TGME49_209970	14.3	20.43	24.36	0.047955	0.226289	1

Table S10. Orthologous NUMTs in *T. gondii* and *N. caninum*

Coordinates of NUMT	Associated nuclear gene	Relationship with associated gene
TGME49_chrV: 1782800-1782918	TGME49_286560 U6 snRNA-associated Sm-like protein	0.9 kb of upstream
TGME49_chrVIIb: 2189430-2189499	TGME49_260520 Hypothetical protein	0.7kb of downstream
TGME49_chrVIII: 1529286-1529361	TGME49_231770 Alpha-tubulin I putative	intron
TGME49_chrIX: 3420407-3420485	TGME49_289740 Hypothetical protein	intron
TGME49_chrX: 3664739-3664832	TGME49_223672 3'(2') 5'-bisphosphate nucleotidase	UTR

Table S11. Amplicons sequencing read data summary

Sample	Raw read pairs	Post trimming			Post merging read pairs			Unique reads			Final total reads
		Paired	R1 single	R2 single	Merged	R1 single	R2 single	Merged	R1 single	R2 single	
WT-1	1 642 096	1 266 572	370 998	1 741	100 100	1 537 470	1 168 213	25 631	198 939	130 903	355 473
WT-2	1 725 362	1 322 225	398 179	2 067	96 027	1 624 377	1 228 265	24 672	227 194	154 273	406 139
WT-3	1 473 826	1 134 113	335 376	1 817	100 691	1 368 798	1 035 239	30 055	214 259	144 393	388 707
Ku80-1	1 465 439	1 284 311	165 356	2 829	12 883	1 436 784	1 274 257	1 621	32 275	24 877	58 773
Ku80-2	1 643 327	1 377 253	176 848	4 989	10 265	1 543 836	1 371 977	907	33 829	23 485	58 221
Ku80-3	1 346 968	1 042 655	131 814	6 145	6 601	1 167 868	1 042 199	667	26 434	21 321	48 422

Table S12. Examples of insertion types observed in amplicons from WT parasites

Insert	Read[a]	Read coordinates		Insert Type	Insert type co-ordinates	
		Insert Start	Insert Stop		Insert Start	Insert Stop
Single mtDNA	M02849:180:000000000-C6C7C:1:1101:19128:17820	58	169	MtDNA Block K	37	148
	M02849:180:000000000-C6C7C:1:1101:19785:3309	68	142	MtDNABlock M	1	75
	M02849:180:000000000-C6C7C:1:1101:21622:18788	56	107	MtDNABlock O	52	1
Single ptDNA	M02849:180:000000000-C6C7C:1:1101:13004:19164	58	232	PtDNA	33724	33546
	M02849:180:000000000-C6C7C:1:1101:11552:15378	50	215	PtDNA	25131	24965
	M02849:180:000000000-C6C7C:1:1101:14358:18348	54	172	PtDNA	31016	30898
Single plasmid DNA	M02849:180:000000000-C6C7C:1:1103:26259:22497	58	232	PlasmidDNA	6039	5865
	M02849:180:000000000-C6C7C:1:1103:26305:17612	59	209	PlasmidDNA	1218	1068
	M02849:180:000000000-C6C7C:1:1103:27169:15635	57	143	PlasmidDNA	7836	7922
Multiple mtDNA	M02849:180:000000000-C6C7C:1:1101:27671:9079	53	88	MtDNABlock K	308	343
		88	137	MtDNA Block J	31	80
		136	171	MtDND Block L	69	104
	M02849:180:000000000-C6C7C:1:1102:29237:16088	58	148	MtDNA Block U	146	56
		145	224	MtDNA Block E	428	349
	M02849:180:000000000-C6C7C:1:1105:17110:1770	62	133	MtDNA Block T	279	208
		127	165	MtDNA Block O	48	86
		166	215	MtDNA Block F	1	50
Multiple ptDNA	M02849:180:000000000-C6C7C:1:1101:15757:22946	55	95	PtDNA	1973	1933
		82	159		34928	34854
		157	225		8818	8886

	M02849:180:000000000-C6C7C:1:1101:13501:14252	56	133	PtDNA	31702	31625
		122	196		30052	29976
	M02849:180:000000000-C6C7C:1:1101:18242:10837	58	112	PtDNA	5225	5171
		109	200		33880	33971
		200	253		17828	17881
Multiple plasmid DNA	M02849:180:000000000-C6C7C:1:1103:27243:20939	58	147	PlasmidDNA	6358	6269
		146	201		6417	6362
	M02849:180:000000000-C6C7C:1:1103:2847:16756	56	161	PlasmidDNA	1478	1367
		124	258		4313	4447
	M02849:180:000000000-C6C7C:1:1103:28737:12687	62	114	PlasmidDNA	3435	3487
		115	184		236	167
		184	251		6327	6260
Multiple insert types	M02849:180:000000000-C6C7C:1:1101:20905:8946	58	196	MtDNA Block L	147	9
		197	260	PtDNA	8070	8133
	M02849:180:000000000-C6C7C:1:1101:14317:17394	58	89	MtDNA Block V	26	57
		90	128	MtDNA Block H	199	237
		129	170	Plasmids DNA	6258	6217
	M02849:180:000000000-C6C7C:1:1101:18961:8446	57	125	PtDNA	57	125
		112	186	PlasmidDNA	112	186
	M02849:180:000000000-C6C7C:1:1102:22648:26257	56	103	PlasmidDNA	6462	6417
		87	135	PlasmidDNA	645	693
		136	182	PtDNA	14402	14448
	M02849:180:000000000-C6C7C:1:1104:20443:21185	58	112	PlasmidDNA	4400	4454
		116	165	MtDNA block T	230	279
		173	248	PtDNA	13011	13086

[a] Reads from WT replicate RH-1

REFERENCES

1. S. Namasivayam *et al.*, A novel fragmented mitochondrial genome in the protist pathogen Toxoplasma gondii and related tissue coccidia. *Genome Res* **31**, 852-865 (2021).
2. J. C. Kissinger, B. Gajria, L. Li, I. T. Paulsen, D. S. Roos, ToxoDB: accessing the Toxoplasma gondii genome. *Nucleic acids research* **31**, 234-236 (2003).
3. A. B. Barrie (2010) Role of Repetitive DNA in Apicomplexan Genome Evolution. in *Biology* (University of Texas at Arlington), p 79.
4. C. Su *et al.*, *Recent exp*ansion of Toxoplasma through enhanced oral transmission. *Science* **299**, 414-416 (2003).
5. J. Sambrook, E. R. Fritsch, T. Maniatis, *Molecular Cloning: A laboratory Manual* (Cold Spring Harbor Laboratory Press, Cold spring Harbor, NY, ed. 2nd, 1989).
6. N. Mullapudi, S. J. Joseph, J. C. Kissinger, Identification and functional characterization of cis-regulatory elements in the apicomplexan parasite Toxoplasma gondii. *Genome Biol* **10**, R34 (2009).
7. L. Sheiner *et al.*, A systematic screen to discover and analyze apicoplast proteins identifies a conserved and essential protein import factor. *PLoS pathogens* **7**, e1002392 (2011).
8. A. M. Bolger, M. Lohse, B. Usadel, Trimmomatic: a flexible trimmer for Illumina sequence data. *Bioinformatics* **30**, 2114-2120 (2014).
9. T. Magoc, S. L. Salzberg, FLASH: fast length adjustment of short reads to improve genome assemblies. *Bioinformatics* **27**, 2957-2963 (2011).
10. R. C. Edgar, B. J. Haas, J. C. Clemente, C. Quince, R. Knight, UCHIME improves sensitivity and speed of chimera detection. *Bioinformatics* **27**, 2194-2200 (2011).